Master's thesis

Magnus Åtland

In-situ measurements of lithium-ion concentrations in a lithium-ion battery using fiber-optical sensors

Master's thesis in Industrial Process Engineering

Supervisor: Jacob Joseph Lamb

Co-supervisor: Markus Solberg Wahl

August 2023

NTNU
Kunnskap for en bedre verden

NTNU
Kunnskap for en bedre verden

NTNU
Kunnskap for en bedre verden

Abstract

In this thesis, a single-mode optical fiber has been implemented into a lithium-ion battery (LiB) to measure the change in concentration in the battery. As the need of energy storage is increasing, due to growth in renewable energy production, a focus is directed toward the research and production of LiB as a proven and promising technology. However, one of the biggest problems of LiB is the lifespan of the batteries, leading to a need for a better knowledge of the capacity changes and the concentration changes of lithium in the batteries. As of now, lithium concentration has been measured *post-mortem*, however, few studies have been done *in-situ*. Therefore, the aim of this study is to measure the change in concentration while the battery is cycling. This will be done based on the changes in the refractive index measured by an optical fiber. The sensor is temperature and concentration calibrated. Then the batteries are cycled through CCCV cycles of C/20, C/10, C/2, 1C, 2C and 3C. The results show the measurements of reflected intensity and concentration could vary depending on several variables but that during cycling a SoC-dependent pattern was formed. This is important because it shows that the sensor is working and can be used to get a better understanding of the change in concentration and capacity.

Sammendrag

I denne oppgaven er en single-mode optisk fiber implementert i et litium-ion batteri (LiB) for å måle endringen i konsentrasjonen i batteriet. Ettersom behovet for energilagring øker, på grunn av vekst i fornybar energiproduksjon, rettes fokus mot forskning og produksjon av LiB som en utprøvd og lovende teknologi. Et av de største problemene med LiB er imidlertid levetiden til batteriene, noe som fører til et behov for bedre kunnskap om kapasitetsendringene og konsentrasjonsendringene av litium i batteriene. Foreløpig har litiumkonsentrasjonen blitt målt *post-mortem*, men få studier er gjort *in-situ*. Derfor er målet med denne studien å måle endringen i konsentrasjon mens batteriet kjører gjennom sykluser. Dette vil bli gjort basert på endringene i brytningsindeksmåling av en optisk fiber. Sensoren er temperatur- og konsentrasjonskalibrert. Deretter går batteriene gjennom CCCV-sykluser på C/20, C/10, C/2, 1C, 2C og 3C. Resultatene viser at målingene av reflektert intensitet og konsentrasjon kan variere avhengig av flere variabler, men at det under syklusene ble dannet et SoC-avhengig mønster. Dette er viktig fordi det viser at sensoren fungerer og kan brukes til å få en bedre forståelse av endringen i konsentrasjon og kapasitet.

Table of contents

1 Introduction

The last decades, the world has seen an increasing focus on climate change, and the use of renewable energy [1]. At the same time, there is a rapid growth in energy demand [2]. To cope with this, many projects using renewable energy are being started all over the world. However, a common disadvantage of renewable energy is the intermittent nature of the power production[3]. One solution to this problem is the use of temporary energy storage through thermal, electrical, mechanical, or chemical systems, or a combination of these. One of the most proven and promising technologies is the Lithium-Ion Battery (LiB) technology [4]. This technology has advantages through a relatively high energy- and power density, and a low self-discharge rate. In addition, it has been proven useful in several ways, such as Plug-in Hybrid Electric Vehicles (PHEVs), Electric Vehicles (EVs), hybrid or fully electric ships, grid energy storage, among many others [5]

In Lithium-ion Batteries, the anodes are typically graphite based, which has the ability to store lithium ions. The cathodes are typically metal oxide based. An organic solvent containing a lithium salt, is typically used as the electrolyte [6].

The Lithium-ion Battery technology faces some challenges with production, due to a high amount of raw materials, and a high energy consumption required. The raw materials required have been identified to be a critical part of the process. Therefore, it is important to address ways to reduce both the energy- and raw material consumption. One way to achieve this, is to extend the lifespan. In this way, less batteries are required to be produced, and less raw materials will be used. To extend the lifespan, battery ageing needs to be reduced. Battery ageing is the loss of capacity over time, or a reduction of State of Health (SoH). One of the main contributors to battery ageing, is the concentration of lithium ions. Throughout the lifetime of the battery, the concentration of available and functional lithium decreases.

1.1 Challenges

This decrease is largely due to the formation of a surface electrolyte interphase (SEI), which contributes to the loss of lithium-ions. SEI itself is important to avoid short circuit and damage to the battery, nonetheless it consumes lithium-ions through the entire lifetime of the battery. Another challenge is the formation of metallic lithium around the anode during charging.

The conventional way of measuring the concentration of lithium-ions today, is to dismantle the battery cell to measure it. However, this method has several drawbacks, e.g. the cell is damaged every time the measurement is performed. Today, there is no proven method that provides the ability to measure the concentration of lithium-ions without opening the cells and damaging them.

Due to the lack of such a method, there is a demand for in-situ detection of lithium, e.g. measuring the concentration of lithium ions during operation with battery charging and discharging. One possible way to achieve this, is by implementing and integrating an optical fiber sensor in the battery cells.

1.2 Literature review

Although studies have been done on optical fibers in batteries, few studies have been done on optical fibers measuring the chemical profiles of the battery. Padilla et al. did a study using a fluorophore (HPNO) which interacted with lithium creating emissive HPNO-Li^+. Light was the absorbed by the fluorophore and a fluorescence spectrum illustrated the connection of the intensity of the emitted light and the increase in concentration of lithium[7]. Nedjalkov et al. manufactured a special Bragg gratings sensor into a separator, sensitive to changes in the refractive index to the electrolyte around [8]. From the study of the Bragg gratings sensor, it was shown that the refractive index of the electrolyte changes as the molar composition of the electrolyte changes. Huang et al. used a tilted fiber Bragg grating optical fiber sensor to measure both the temperature and the state of the electrolyte as the battery was cycling [[9]].

1.3 Aims of the study

The aim of this thesis is to measure the change lithium-ion concentrations in a lithium-ion battery by using a fiber-optical sensor and the Fresnel equation through the refractive index of the fiber and the electrolyte outside of the fiber. This was chosen because of the least number of variables as it does not include measures of strain or fluorophore. Limitation of this scope is that the measured volume cannot be expected to perfectly represent the electrolyte between the electrodes as without the sensor. All measurements will be done live (in-situ) during charging and discharging. The thesis will include implementation of fiber-optical sensors in batteries, concentration and temperature calibrations of the sensor, wetting and formation cycles of the batteries and monitoring the state-of-charge (SoC) dependent concentrations of the lithium-ions in the electrolyte while running different c-rate tests.

2 Theory

This chapter introduces the working principle of of LiBs, their battery chemistry, as well as ageing mechanism related to LiBs. An introduction to optical fiber sensors and the most common types of these is then presented, with a focus on how these can be used to measure the lithium-ion concentration in LiBs. The basis for this theory has been developed from my project report delivered earlier in my 5th year of study [51].

2.1 Lithium-ion Batteries

A lithium-ion battery (LiB) cell consists of two electrodes (an anode and a cathode), a separator, electrolyte and current collectors for the two electrodes, which is illustrated in Figure 1. The anode usually consists of graphite or carbon in different structures or a combination of graphite and other materials, which, during a discharge of the battery, has the ability to transit and release a lithium through the electrolyte and to the other electrode. This report has a focus on lithium intercalation batteries. These are batteries where lithium-ions intercalate into the structure of the electrodes [10]. The lithium is transported from the structure inside one electrode to inside the structure of the other electrode during charging/discharging. In Figure 1 one can see that in pure graphite a structure of 6 carbons is needed to store one lithium ion. Between the electrodes there is a separator that allows the lithium ions to flow through, however its main purpose is to prevent the electrodes from physical contact with each other and accordingly to prevent a short-circuit [10]. The free electrons released when the lithium ions are released form the anode, will travel through the current collectors in an external circuit to the other electrode. The reason of this behavior is because the electrolyte is an insulator, and the current collector has a high electrical conductivity. The most commonly used current collectors in LiBs are aluminum for the cathode and copper for the anode [11]. The cathode is based on a transition metal oxide. The metal is chosen on behalf of its ability to release, receive and store lithium ions.

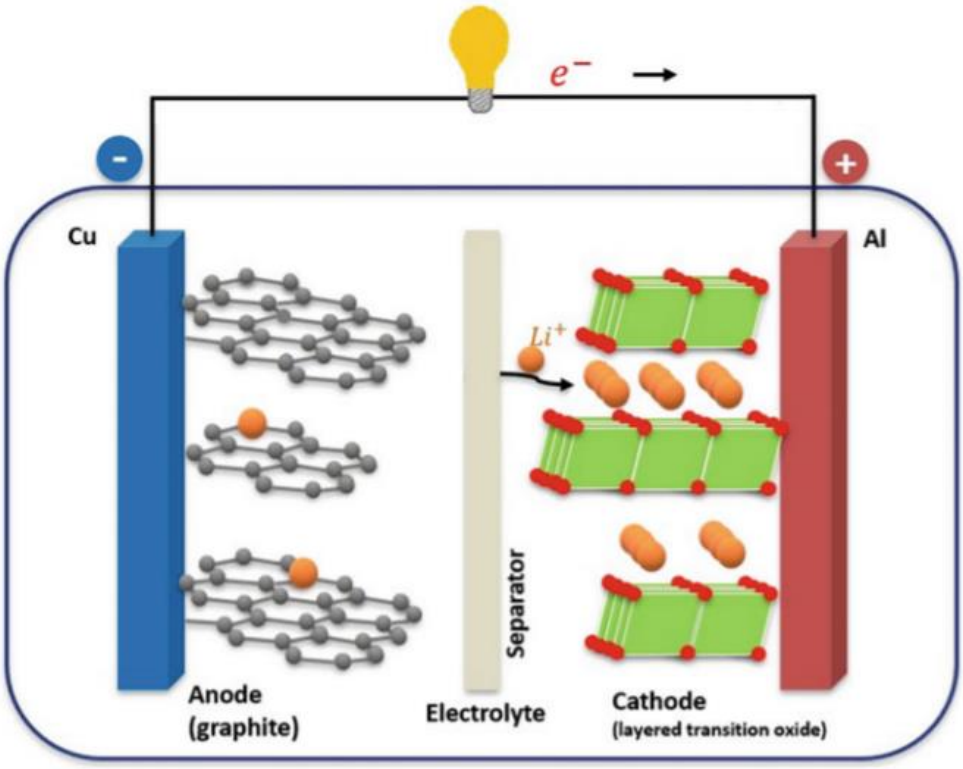

FIGURE 1: WORKING PRINCIPLE OF A LIB. THE BATTERY IS DISCHARGING, WHERE LITHIUM IONS INTERCALATE FROM THE ANODE TO THE CATHODE. ONE IS STORED BY SIX CARBONS IN THE ANODE BEFORE THEY MOVE THROUGH THE SEPARATOR TO THE LAYERED STRUCTURED CATHODE. THE ELECTRONS FLOW IN AN EXTERNAL CIRCUIT [10].

For a LiB to work, and the lithium ions to intercalate back and forth from the cathode to the anode, the material in electrodes must change their oxidation numbers [11]. One electrode must increase its oxidation number while the other electrode must decrease its oxidation number. When discussing batteries, it has been defined to talk about batteries when they are discharging. During a discharge, the electrode where an oxidation reaction happens and the oxidation number increases will always be referred to as the anode (from Greek: “way up”, ana- “up” and hodos- “way”) [12]. While at the electrode where the oxidation number decreases and therefore the reduction reaction happens will always be referred to as the cathode (from Greek: “way down”, kata- “down” and hodos- “way”). During a charge, the oxidation reaction will happen in the cathode while the reduction reaction will happen in the anode. The potential difference between the electrodes due to the oxidation and reduction reactions defines the spontaneous flow of ions and electrons, as discussed in the paragraph above.

2.2 Battery chemistries

The electrode materials used in the battery are the most important components to characterize the battery and giving its attributes. The following section will discuss the most common anode and cathode chemistries.

2.2.1 Cathode chemistries

The most common cathode materials in a LiB are transition metal oxides, which have structures and ability to store guest ions. These chemistries must be able to easily change their oxidation number to be able to release and receive lithium ions. Therefore, the most common cathode materials consist of manganese, iron, cobalt or nickel. The common denominator for these metals is that they are relatively light, and they all have partially filled d-orbitals, making them flexible as to changing their oxidation numbers [11]. Different structures and combinations of these result in a variation in different important properties. For example, their ability to intercalate lithium ions, voltage, capacity, thermal stability, volumetric energy density and gravimetric energy density.

TABLE 1: AN OVERVIEW OF THE MOST COMMERCIAL CATHODE MATERIALS [13].

LIB Chemistry	Year	Advantages	Applications
Lithium Cobalt Oxide ($LiCoO_2$)	1991	High specific energy	Broad use
Lithium Iron Phosphate (LFP, $LiFePO_4$)	1996	Moderate density (2Ah outputs 70A) High safety operating temperature >60℃	Personal Transport, power tools, aviation products, automotive hybrid systems, PHEV conversions, low range EVs
Lithium Manganese Oxide (LMO, $LiMn_2O_4$)	1996		Hybrid EV, mobile phone, laptop
Lithium Nickel Cobalt Aluminum Oxide (NCA, $LiNiCoAlO_2$)	1999	High specific energy, good life span	Battery EVs
Lithium Nickel Manganese Cobalt Oxide (NMC, $LiNi_xMn_yCo_zO_2$)	2008	Good specific energy and specific power density	Battery EVs, power tools, grid energy storage

Lithium Cobalt Oxide (LCO) was first commercially made by Sony in 1991. LCO has a layered structure allowing the electrons to easily transition out of the cathode. LCO is still broadly used as a cathode today, making it the most commercially successful cathode among LiBs with layered structure. LCO is known for its high specific energy, high specific capacity and high volumetric capacity. However, it has a low thermal stability, which increases the risk of thermal runaway, meaning that when the battery is heated to a certain point it just keeps getting warmer until it eventually can burst into flames [14]

Lithium iron phosphate (LFP) is a very common cathode and is a cathode often used in car batteries. It has an olivine structure, which strengthens, along with iron, its stability and safety. It is also known for its high-power capability [15].

Lithium manganese oxide (LMO) has a spinel structure. Compared to the material in LCO, manganese is much cheaper and less toxic than the cobalt in the LCO. However, it has some unwanted features as a structural change and dissolution of manganese during cycling[16]. To cope with this problem, one can repress it different strategies like surface coating of ZnO or metal doping [17], [18].

Lithium nickel cobalt aluminum oxide (NCA) is a layered structured cathode most known in Panasonic batteries used in Tesla EVs [19]. A high amount of nickel in the cathode is beneficial, because it contributes to a high energy density. However, too much nickel has been proven to block lithium ions path back into the cathode, and instead take the lithium's place. To control this cobalt is included in the cathode material. A little bit of aluminum is included to strengthen the cathodes thermal stability [20].

Lithium nickel manganese cobalt oxide (NMC) has much of the same characteristics as NCA. Nickel contributes to high energy and power densities and provides high lithium extraction, while manganese and cobalt contributes to more stability, safety and cycle life [21]. NMC has proven to have very good attributes and can be tailored to different strong attributes. Different compositions of material in the cathode can result in high energy density, high power density or high specific capacity, depending on what is required. As a higher concentration of nickel often leads to higher energy/power density, while a composition with more cobalt and manganese often leads to more safety and stability.

2.2.2 Anode chemistries

The optimal anode material would have been metallic lithium, because of its low electrode potential. However, lithium metal may create branches (dendrites) extending out of the metal, which may pierce the separator and short circuit the cell. This can lead to a thermal run-away and start a fire. Therefore, other anode materials have proven to be important in a LiB.

Today, graphite is the anode material of choice in most batteries. This material can store up to one lithium ion per six carbon atoms. Carbon is a very good material because of several reasons. It is easy to get and cheap because of the amount and availability of it on earth [22]. It has a high lithium diffusivity, electrical conductivity as well as a great mechanically stability where it has a low volume expansion during lithiation, compared to other materials. However, it is heavier and therefore has a higher gravimetric capacity. Another disadvantage is that the (de-)intercalation causes strain to develop in the graphite. This strain can damage the solid-electrolyte interface (SEI) layer and reduce the battery lifespan [23]. The SEI layer consumes lithium throughout the lifetime

of the battery, concluding in loss of capacity of the battery. The SEI will be explained further in the following section.

Another carbon anode material is hard carbon. As graphite is layered and stacked, hard carbon is randomly stacked and does not have a fine structure as graphite. This results in a higher capacity, higher cycle life and lower expansion. However, hard carbon has a lower density due to the void spaces, which results in a lower volumetric capacity compared to graphite. The main disadvantage compared to hard carbon is the increase in development of the SEI due to exposed edge planes from the structure of the anode [24].

Silicon has also been used as an anode material. It demands less space than a carbon anode and it is lighter, which significantly increases the energy density of the batteries. However, silicon expands up to 300% during lithiation, which can be problematic. To solve this or reduce the expansion, combinations of silicon and carbon anodes have been made. Lithium titanium oxide is another material used as an anode. Compared to the carbon, it has a higher volumetric capacity, better thermal stability, higher cycle life and a higher rate. However, it has a lower capacity and a reduced cell voltage. Titanium is also more expensive than carbon [15].

2.2.3 Electrolyte

An electrolyte that contains Li-ions allows for their transportation between the electrodes. Typically, electrolytes are composed of a lithium salt, such as LiPF6 or LiFAP, and two or more organic solvents [25]. In many cases, a combination of solvents and salts is necessary to ensure that the electrolyte has all the required properties for use in batteries. To fulfill all of the necessary requirements, additional additives may be included in the electrolyte to make it non-flammable and to prevent overcharging. Important properties that impact the performance of the battery include high ionic conductivity, a broad electrochemical stability range, and low electrical conductivity [26]. High ionic conductivity allows for easy transportation of Li-ions between and through the electrodes while also preventing polarization and high overpotentials. A broad stability window prevents that the electrolyte does not degrade or react with electrode components, even when cycled at varying voltages. A low electrical conductivity minimizes the self-discharge rate and maximizes capacity.

2.2.4 Separator

The separator is a physical barrier between the anode and cathode that prevents them from making direct contact. It is designed to permit the flow of Li-ions through its porous structure while being electronically insulating to prevent battery self-discharge. Besides, the separator must exhibit chemical and mechanical stability and serve as a safety measure to prevent thermal runaway. Polyethylene (PE), polypropylene (PP), and a combination of the two are commonly used separator materials due to increase safety [27]. Commercial separators often comprise PP-PE-PP trilayers, where the low melting point of PE enables it to fill the electrode pores, which increases battery resistance and hinders further operation. Moreover, the higher temperature

stability of PP than PE helps to avoid short-circuiting of the battery in cases of uncontrolled temperature increases.

2.3 Battery aging and degradation

As mentioned, there is a demand for energy storage with the increasing production of renewable energy, and LiBs can be a solid solution to this demand. However, there are limitations, such as ageing mechanisms that reduces the lifetime for the battery. Ageing mechanisms are often divided into three categories, loss of lithium inventory (LLI), loss of active material (LAM) and impedance increase.

The development of the SEI layer is the most influential contributor to the LLI [28]. The SEI layer is formed during the first cycles of the battery, called formation cycles, which are performed by the battery manufacturer. Lithium is converted around the carbon particles in the anode, creating a passivating layer. The SEI layer continues to grow during cycling of the battery, and especially if the anode expands and damages the SEI layer, results in more cyclable lithium ions consumed by the SEI layer and therefore less capacity in the battery [10]. Even though the SEI layer reduces the amount of lithium-ions and therefore the battery capacity, it is necessary for the lithium-ions to be able to enter the anode.

Another reason for LLI is lithium plating. When the temperature falls below the recommended operating range, the rate of degradation mechanisms in a lithium-ion battery (LIB) increases. Among these mechanisms, the most significant aging process is lithium metal plating. This risk of plating is aggravated by low lithium diffusion into the graphite anode and high charging rates at low temperatures. As a result of lithium plating, some Li-ions are lost irreversibly during the process, leading to a decrease in capacity and making them unavailable for charge transportation in the battery [29]. This phenomenon has both immediate and long-term effects on the capacity and charging rate of the battery, resulting in a decrease in capacity due to the loss of lithium.

An ageing mechanism related to LAM is dissolution of material. This can happen when using a propylene carbonate-based electrolyte with a graphite anode [30]. The electrolyte follows the lithium into the anode and consequently exfoliate the carbon. As well as using the electrolyte lithium hexafluorophosphate also includes some hydrofluoric acid, which dissolves the electrode materials. This results in passivation in the electrode as well as increased thermal resistance [31]. Another example of LAM is structural degrading. This can take place in different ways depending on the chemical compositions of the electrodes [32]. One way is by the exposure of too high temperature. This results in less space for the lithium ions in the electrodes, limiting the effective storage capacity.

With the increase of impedance, the concerns are mainly with the increase of ionic resistance in the battery. Common reasons why impedance occur are passivation of active material and conductivity losses [33].

2.4 Sensors

In general, a sensor is a device sends a signal in response to changes in its surroundings. It is important that the sensor is sensitive to a few, ideally only one, but important parameters and are not affected by the other parameters. Likewise, it is also important that the sensor do not affect or impact the operation of what it is measuring. For usage of sensors in batteries, it is important that they are small and electrically insulating. Therefore, fiber optic sensors are often considered an ideal solution.

2.4.1 Fiber optic sensors

Optical fibers are cylindrical tubes often made of silica, where photons travel through the core of the fiber. The core of the optical fiber has high enough refractive index for the core to have total internal reflection, which means that all the light is reflected when it hits the wall of the core. Sensors based on optical fibers can measure parameters such as temperature, pressure and chemical concentrations [34]–[36]. The ability to measure such parameters, as well as having a very low conductivity, volume and weight, and being chemically inert, makes it optimal as sensors in batteries.

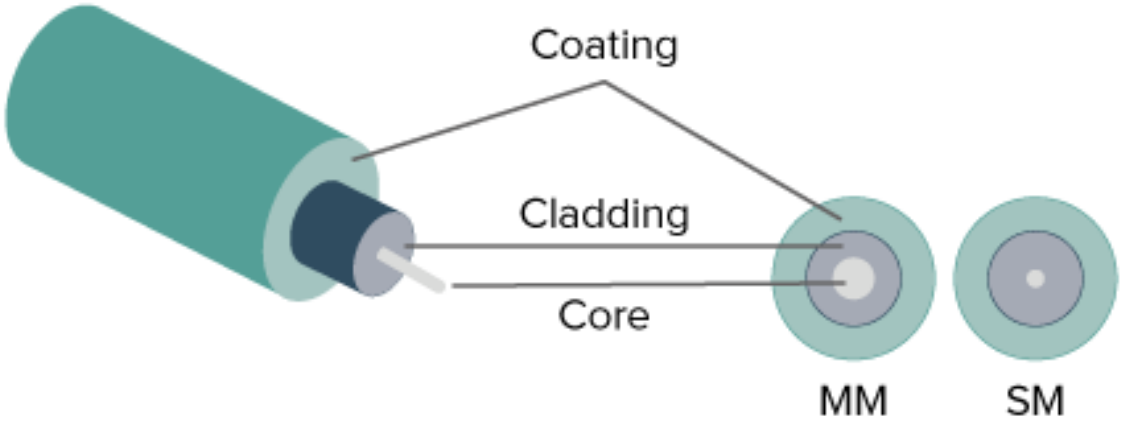

FIGURE 2: AN OPTICAL FIBER SENSOR. THE FIGURE SHOWS THE CORE, CLADDING AND COATING OF A MULTIMODE AND A SINGLEMODE FIBER [53].

In the general setup of an optical sensor the input signal comes from a light source and goes through the fiber, where the signal is changed by the environment. From here the signal is captured by the detector and though data processing the parameters we wanted to measure can be detected.

There are several types of fiber optical sensors, e.g., interferometric sensors, distributed fiber-optic sensors, fiber optic temperature sensors and refractive index sensors [37]–[40].

2.4.1.1 Interferometric sensor

Interferometric sensors are an important class of sensors that measure the interference between two or more waves. This type of sensor requires the light to be split into multiple paths to create interference patterns. There are different types of interferometric sensors available, and each has its unique way of generating interference patterns. Two examples of these sensors are multi-mode interferometers and fiber Bragg gratings (FBG) [41], [42].

A multi-mode interferometer generates interference patterns by utilizing the different modes of the light that have varying velocities within an optical fiber [43]. This difference in velocity leads to interference, which can be used to measure temperature changes within the fiber due to thermal expansion or the thermo-optic effect. The thermo-optic effect refers to the changes in the refractive index of the fiber that occur due to changes in temperature. These changes in the interference pattern can be measured to determine the temperature changes.

Fiber Bragg gratings are another type of interferometric sensor that utilizes the variation of refractive index in the core of an optical fiber. This variation creates a constructive interference that reflects a specific wavelength. This reflected wavelength is sensitive to changes in strain and temperature. As the strain or temperature changes, the reflected wavelength changes as well, providing a measurement of the change.

2.4.1.2 Refractive index sensors

Refractive index sensors are used to measure the refractive index. The refractive index is a measure of how much the light bends or slows down though a medium. It is defined as the speed of light in vacuum divided on the speed of light through the medium and is denoted by the symbol “n”, as shown in equation 1. The refractive index of a material depends on its chemical composition and its physical properties, such as density and temperature. There will therefore be a difference in the refractive index of the electrolyte when changing the concentration of the lithium in the electrolyte.

$$n = \frac{c}{v} \tag{1}$$

When guiding the light through the fiber to the surroundings we look at the intensity of the reflected light to measure the refractive index. The Fresnel equations is a set of equations that describe how light is reflected and

transmitted at the boundary between two media with different refractive indices. By using an optical fiber, we can assume that the light is incident at perpendicular angle to the medium outside of the fiber, resulting from the small radius of the inner core of the fiber. When the angle of incidence is 90 degrees the Fresnel equation simplifies considerably. The reflected signal intensity is described by the Fresnel equation [44]:

$$R = \left(\frac{n_f - n_m}{n_f + n_m}\right)^2 \quad (2)$$

Here R is the reflectivity, n_f is the refractive index of the medium in the core of the fiber and n_m is the refractive index of the medium around the fiber. The graph shows the Fresnel equation tested on the medium. The reflected intensity goes towards zero when n_m is equal to n_f.

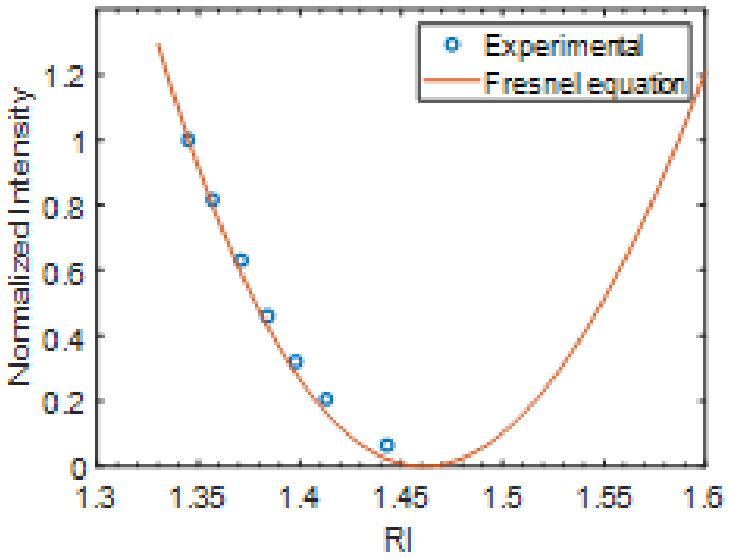

FIGURE 3: THE FIGURE SHOWS THE EXPERIMENTAL RESULTS COMPARED TO THE FRESNEL EQUATION. THE FIGURE IS FROM PREVIOUS EXPERIMENTS CONDUCTED IN THE GROUP.

2.4.1.3 Fiber Bragg-grating sensors

Fiber Bragg-grating (FBG) sensors are widely used for measuring temperature using optical fibers, as they are the most widely available and easiest option [16]. They have a linear sensitivity to both temperature and strain, with the main source of error being the cross-sensitivity between the two. The sensitivity of FBGs is typically around 10 pm shift in wavelength per degree Celsius. However, it is important to note that ordinary FBGs are optimal for measuring temperatures up to 200°C before significant degradation occurs [17].

FBGs can also be used for measuring other parameters by incorporating stimuli-responsive coatings. For example, in Figure 4e, a tilted FBG is used as a refractive index sensor by guiding light out and allowing it to interact with the surrounding environment. This allows for the measurement of changes in the refractive index, which can provide information about various parameters such as humidity, pressure, and chemical composition.

Additionally, FBGs can be used in a wide range of applications due to their small size, high sensitivity, and immunity to electromagnetic interference. They can be used in structural health monitoring for bridges, buildings, and aircraft, as well as in medical and biological sensing applications.

2.4.1.4 Distributed sensing

Distributed fiber optical sensors measure the temperature or strain along the whole fiber. The backscattering in the fiber will be affected by the strain or temperature on the fiber [45]. The location in the fiber where the signal originates can be calculated based on a time-of-flight principle, which requires a pulsed light source.

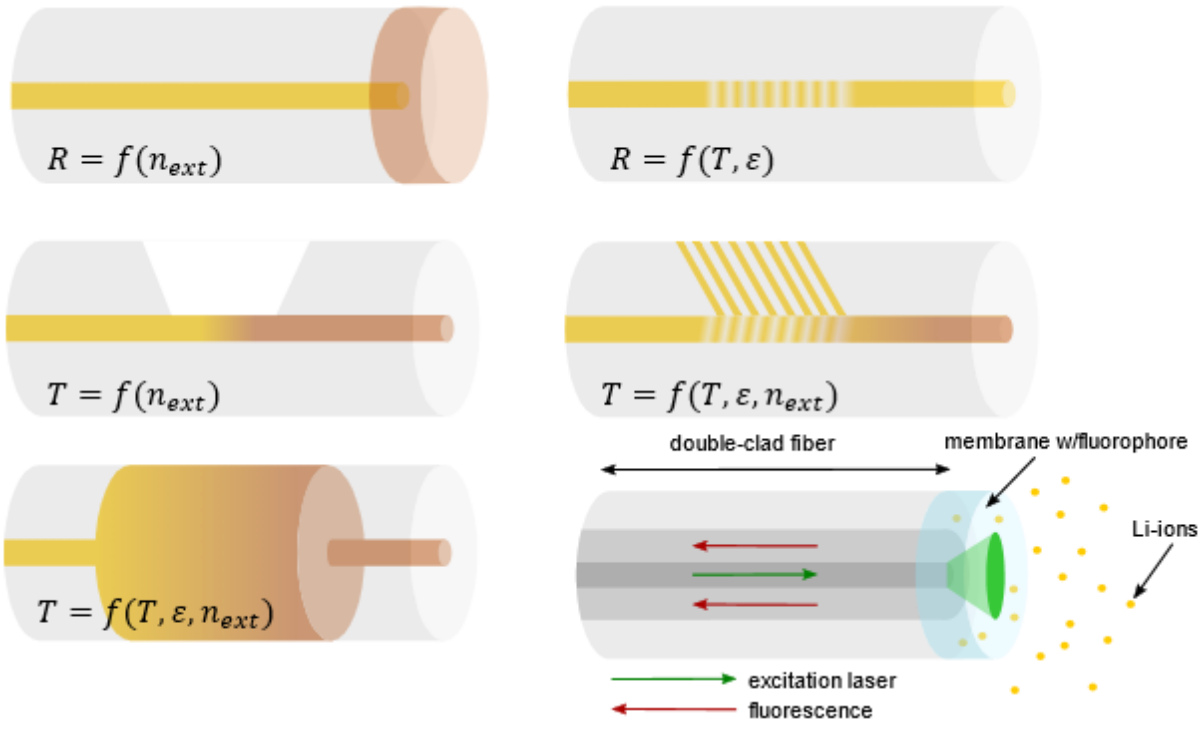

FIGURE 4: DIFFERENT TYPES OF OPTICAL FIBERS. A) IS AN END-FACE SENSITIVITY OPTICAL FIBER AND CAN BE USED AS A REFRACTIVE INDEX SENSOR AS IT IS IN CONTACT WITH THE SURROUNDINGS. B) IS A D-SHAPED OPTICAL FIBER AND CAN ALSO BE USED AS A

REFRACTIVE INDEX SENSOR. C) IS A MULTIMODE INTERFEROMETER. D) IS A FIBER BRAGG GRATING OPTICAL FIBER. E) IS A TILTED FIBER BRAGG GRATING OPTICAL FIBER. F) IS A DOUBLE-CLAD FIBER TO EXCITE AND CAPTURE FLUORESCENCE [54].

2.4.1.5 Fluorescence fiber optic sensors

The theory behind the fluorescence-based optical sensor is generally that light is guided by the fiber to the environment, where the environment absorbs the photons and emits the back with a different wavelength. This sensor setup will be discussed more thoroughly in the next section. The fiber measures these wavelengths for us to get a better understanding of the environment. The optical fiber most used in this experiment is called a double-clad fiber. This fiber has a core where the light is guided from the light source to the tip of the fiber, and a larger diameter section (the inner cladding) outside of the core that collects the emitted light from the surroundings [46].Figure 5 shows the refractive index on the y-axis and the radius as the x-axis for a double clad fiber. This means that the light does not escape from the core to the inner cladding, and the emitted light goes straight through the core from the inner cladding. The other optical fiber used in the experiment is a bifurcated fiber, which is two fibers next to each other or a fiber with two cores, one guiding the light from the light source to the soundings and one collecting the emitted light.

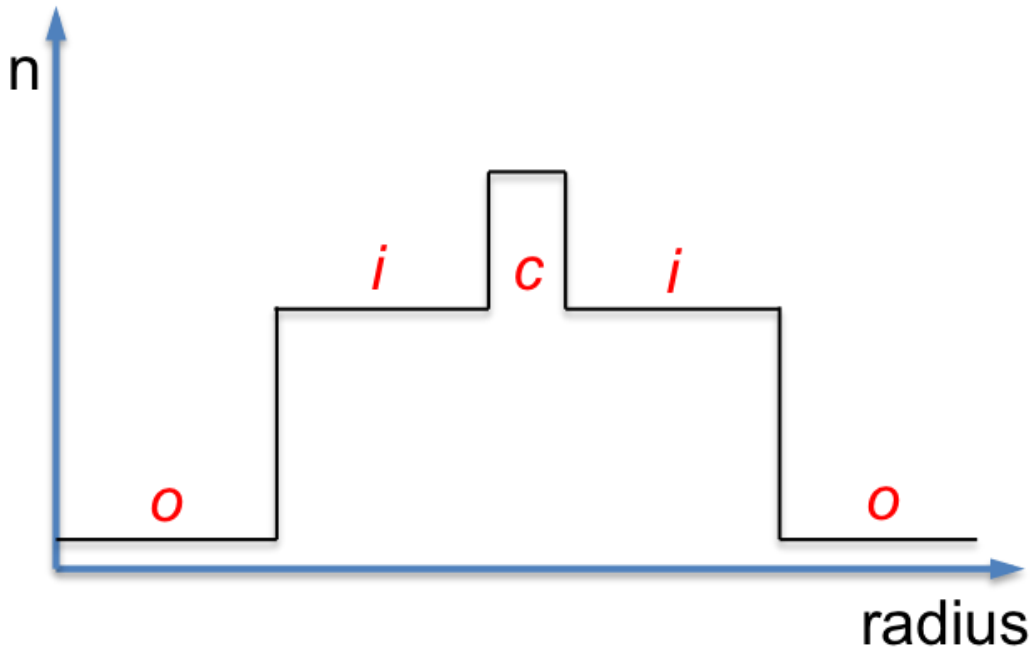

FIGURE 5: A REFRACTIVE INDEX GRAPH OF A DOUBLE-CLAD FIBER. THE Y-AXIS IS THE REFRACTIVE INDEX, WHILE THE X-AXIS IS THE RADIUS OF THE FIBER.

Fluorescence fiber-optic sensors can be made with a small diameter, allowing them theoretically to be able to be inserted in a battery with minimal effect on the battery operation. With immobilized fluorophores attached to the fiber, detection of chemicals concentrations is possible. This allows for continuous monitoring of a battery, without interfering with either the package or the chemical environment in the battery.

3 Experimental

3.1 Setup

The experiments are an extension of an earlier article by [52], in which an almost identical setup was used. The setup is shown in Figure 6. The setup consists of 4 main parts, namely the lithium-ion battery (1) under test, the fiber-optic sensing interrogator (2), the hardware connections between the battery and the interrogator (3), and the temperature chamber (4).

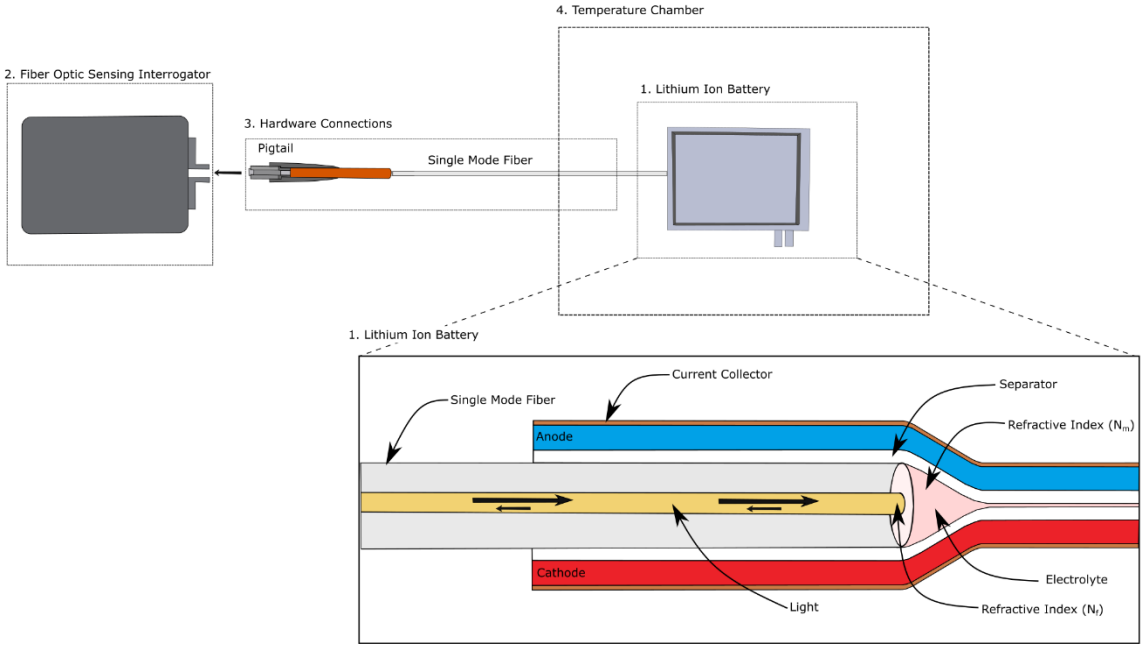

FIGURE 6: EXPERIMENTAL SETUP. THE SETUP CONSISTS OF 4 MAIN PARTS, NAMELY THE LITHIUM-ION BATTERY (1) UNDER TEST, THE FIBER-OPTIC SENSING INTERROGATOR (2), THE HARDWARE CONNECTIONS BETWEEN THE BATTERY AND THE INTERROGATOR (3), AND THE TEMPERATURE CHAMBER (4). THE LITHIUM-ION BATTERY DRAWING IS INSPIRED BY [52]

The batteries selected in this thesis are lithium intercalation batteries and the sensor measures the changes of lithium in the electrolyte situated between the cathode and the anode. The battery chosen was NMC111/graphite. This is because NMC (Nickel Manganese Cobalt) has an increasing focus in scientific research papers [47], [48]and can be tailored for many uses, depending on the need for specific energy and specific power density [47]. The lithium-ion battery was modified to allow real-time measurements. For this purpose a single-mode fiber (SMF-28, 125 µm) was placed between the electrodes of an NMC111/graphite pouch cell (200 mAh LiFun, China). An additional separator was placed between the fiber and the electrode to have separator material and the same distance between the fiber and both electrodes. The implementation procedure can be found in chapter 3.2. After sealing, the cell was wetted. This process distributes the electrolyte throughout all

components of the battery to allow the lithium to move freely from one electrode to the other. After wetting, the battery goes through a formation cycle. The wetting and formation process is described in chapter 3.4. After formation, the battery was tested as described in chapter 3.5.1 to ensure the battery was fully functional before testing the sensor. The fiber was spliced to a fiber pigtail to connect it to the experimental setup as shown in Figure 6. The fiber optic sensor interrogator is of the type HYPERION si255. The sensor interrogator includes a laser and a spectrometer as shown in Figure 6. The wavelength chosen is in the infrared spectrum and was set at 1500 nm. It was tested up to 1600 nm with 10,000 points in between. The wavelength accuracy of the interrogator is 2 pm with a wavelength stability of 3 pm.

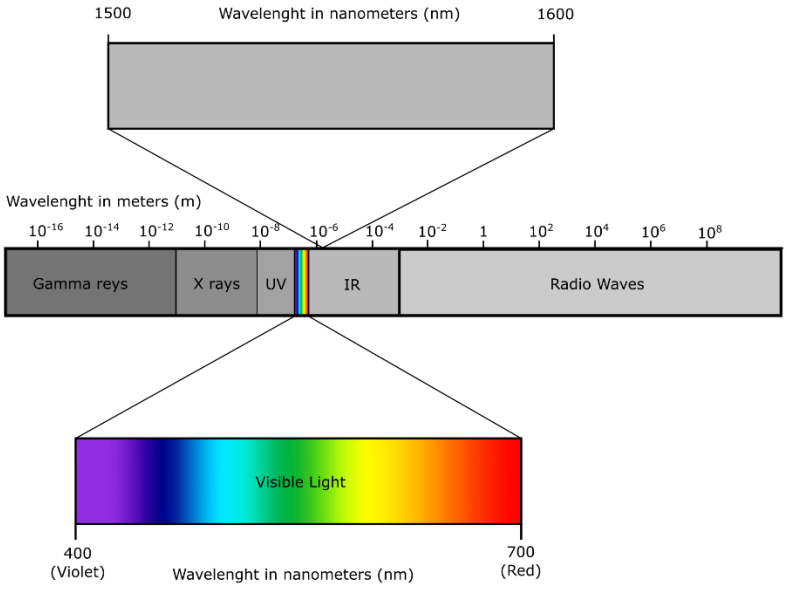

FIGURE 7: THE FIGURE SHOWS THE APPLICABLE WAVELENGTH SELECTED FOR REAL TIME MEASUREMENTS OF THE LITHIUM ION BATTERY. IT IS EVIDENT FROM THE ILLUSTRATION THAT THE WAVELENGTH IS WITHIN THE INFRARED SPECTRUM AT A WAVELENGTH OF 1500 – 1600NM. THE FIGURE IS INSPIRED BY [49]

3.2 Implementation procedure

Batteries of type NMC111/graphite pouch cells (200 mAh LiFun, China) are presented in this work. Before implementing the fiber into the battery the original pouch was removed from the battery. The first step in the fiber implementation process involves fabricating a new pouch for the battery. This is done by using a stamp one of the sides of the pouch that is of the size 4.5 x 6 cm. This serves to efficiently support the placement of the battery and to have more successful sealing over the collectors. The fiber and separator were then carefully placed into one side of the battery before sealing the sides of the pouch using a heating sealer (Magneta 421 MG, heat level 6) and the pouch over the collectors using a straightener (Remington S1005, 180°C).

TABLE 2: THE STEP-BY-STEP PROCEDURE FOR INTEGRATING THE FIBER INTO THE BATTERY.

Step	Action	Details
1.	Production of new pouch consisting of two identical 7 x 18 cm pouch material.	
2.	Removal of the original pouch in battery.	Try to remove as much pouch material as possible around the collectors as this is the most crucial part for good sealing.
3.	Stamp one side of the new pouch to fit battery.	The stamp is placed at the edge of the pouch in such a way that there is 0.5 cm from the stamp to the top of the pouch, 2 cm to the bottom of the pouch and 3 cm to the end of the short side of the pouch.
4.	Repacking the battery into the new pouch assembly.	Use Kapton tape (polyimide) to make the battery stay put to the new pouch.
5.	Adding black polymer tape (EQ -PLIb-HMA4-L200) between the battery collectors and the pouch.	It is important that the polymer tape is above the pouch, as the battery will short circuit if the collectors touch the edge of the pouch and not the polymer tape.
6.	Adding black polymer tape between the fiber and the pouch.	This is done to get a better seal, so there will be no leakage at the fiber.
7.	Remove cladding at the end of the fiber and using a cleaver for straight cut on the fiber.	Clean the end of the fiber with ethanol before using the cleaver.
8.	Add extra separator between the fiber and the open electrode.	
9.	Insert the optical fiber into the battery at the opposite side of the collectors.	Use Kapton tape (polyimide) on the fiber at the non-stamp pouch side, to make it stay put during vacuum sealing, so the fiber will not break.
10.	Assembly of two pouch sides.	

11.	Using Heating Machine to melt one of the short sides of the pouch (closest to battery).	This is done to easier seal at the collectors and fiber without getting a bend and small opening in the pouch, and consequently a leakage.
12.	Using straightener to close pouch side above collectors.	This step is crucial as a mistake here will lead to poor sealing and leakage. Use the straightener just over the collectors. It is important that the pouch material align and is straight (no bend). Use the straightener for 5 seconds twice.
13.	Use Heating Machine to melt sides where the fibers and collectors are located.	Seal the rest of the side with the collectors and the side where the fiber is. Use it twice over the fiber to ensure a good seal.
14.	Insert battery into Glove Box filled with argon.	Keep it in the vacuum box before entering the Glove box for 12 hours to remove moisture.
15.	Add electrolyte (1M LiPF6 in EC:DMC (50:50)) into the open pouch side within the Glove Box.	Try to add the electrolyte close to the battery for a faster wetting. Add 1.15 ml electrolyte. This is 115% of the recommended volume from the cell information. This was to ensure a good wetting as this pouch is bigger than the original commercial pouch.
16.	Move battery from working space to vacuum chamber (AUDIONVAC VMS 53) within the Glove Box.	
17.	Close lid, and wait 20 seconds for the battery to be vacuum sealed.	

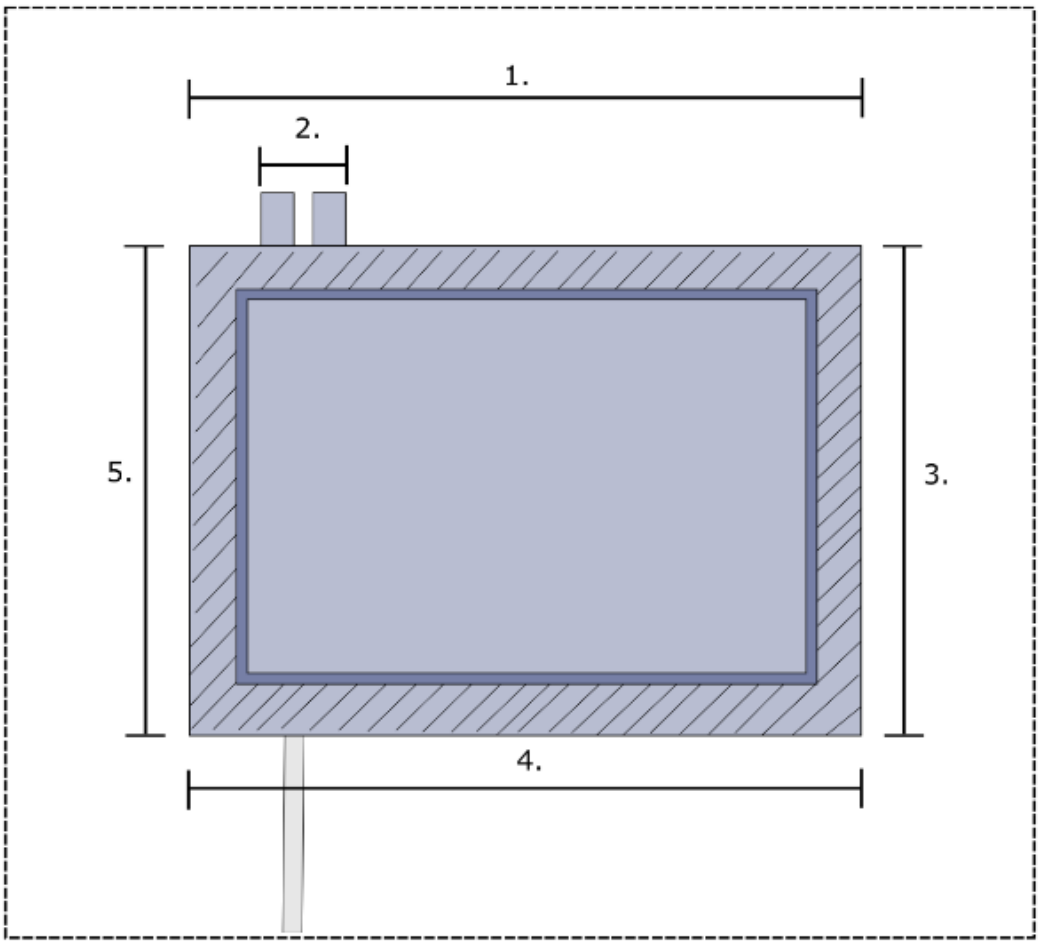

FIGURE 8: THE FIGURE SHOWS THE BATTERY AFTER SEALING THE POUCH. SIDE NR. 1 IS THE SIDE WHERE THE COLLECTORS ARE PLACED. AREA NR. 2 IS ABOVE THE COLLECTORS. SIDE NR. 4 IS WHERE THE OPTICAL FIBER IS PLACED. SIDE NR. 5 IS THE SHORT SIDE CLOSE TO THE BATTERY WHICH IS SEALED VERY FIRST. SIDE NR. 3 IS THE SIDE WHERE ELECTROLYTE IS INSERTED.

3.3 Calibrations

3.3.1 Concentration calibration

The objective for the concentration calibration of the optical fiber is to measure the intensity of the reflected light when the concentration of the electrolyte (1M LiPF6 in EC:DMC (50:50)) is changed from 1M to 0.9M, 0.8M and finally 0.7M. The pouch material was cut to the size of 16 cm x 20 cm and then folded to 8 cm x 20 cm. The outer cladding of a single mode fiber was removed at the end of the fiber and a cleaver was used to get a straight cut on the fiber. Then the fiber was inserted into one of the short sides of the pouch and black polymer tape was placed between the fiber and the poach to ensure a good seal. The two short sides were sealed with a heat sealer. Clamps and plexiglas were used to create four pockets in the pouch. The long side was sealed with a straightener so that a pipette could fit into each pocket to insert electrolyte. The pouch was then placed in a glove box filled with argon. 1 ml of electrolyte, 0.111 ml, 0.139 ml and 0.179 ml of DMC were inserted into the pockets from the fiber and into the other short side respectively. The long side was completely sealed in the

glovebox with a vacuum chamber. The test was done by holding the pouch in a fixed position. During the concentration calibration, the clamp and plexiglas near the fiber were removed every two hours, so that the concentration of the electrolyte in front of the fiber changed from 1 M to 0.9 M, 0.8 M, and then 0.7 M. The single mode fiber was spliced to a pigtail fiber connected to a fiber optic sensing interrogator (HYPERION si255 Fiber Optic Sensing Interrogator). The result was analyzed and stored by Sensing Analysis Software ENLIGHT (version 1.18.8.0) by plotting intensity (dBm) per wavelength (nm). Every 2.5 minutes, 10000 points of intensity were stored between wavelengths 1500 nm and 1600 nm with a delta of 0.01 nm. The result was implemented in a MATLAB script where the average of all 10000 points per time was calculated and a graph of intensity per time was generated. A MATLAB script was then used to calculate a calibration line by using a best fit line formula. The points used in the best fit line formula was an average of the stable period before a change in concentration. The script can be found in the Appendix 7.1. The calibration was performed twice.

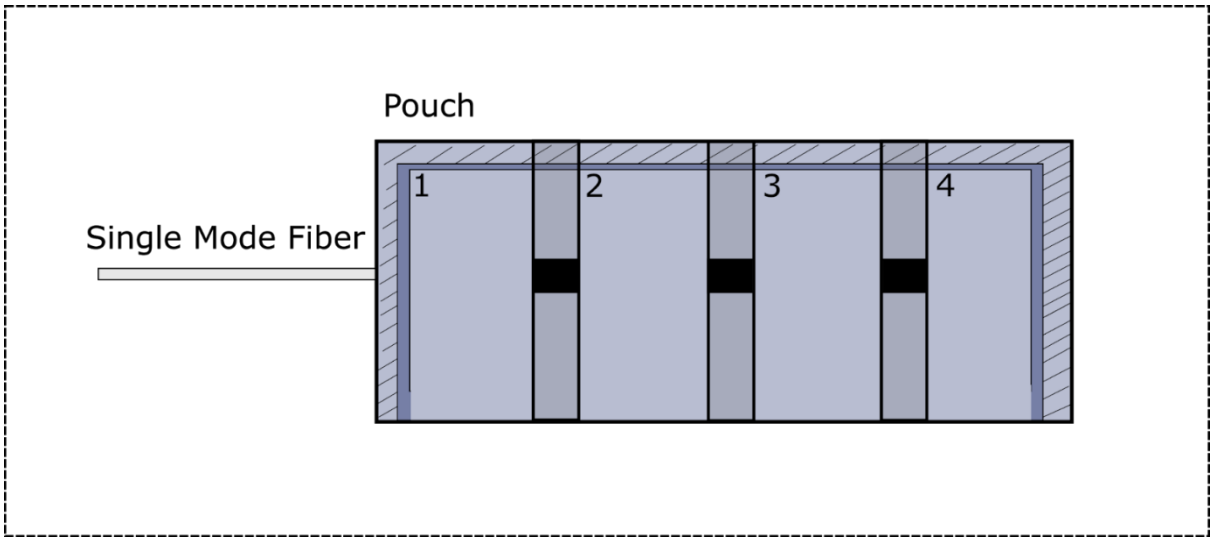

FIGURE 9: THE POUCH USED FOR THE CONCENTRATION CALIBRATION OF THE SENSOR. THE DIFFERENT NUMBERS REPRESENT THE DIFFERENT POCKETS. POCKET NR. 1 HAS 1 ML OF 1 M $LiPF_6$ IN EC:DMC (50:50), POCKET NR. 2 HAS 0.111 ML OF DMC, POCKET NR. 3 HAS 0.139 ML OF DMC AND POCKET NR. 4 HAS 0.179 ML OF DMC. THE POCKETS ARE SEPARATED BY TRANSPARENT PLEXIGLAS WITH CLAMPS CONNECTED TO THEM (THE BLACK SQUARES) TO TEMPORARILY SEAL THE AREA BETWEEN THE POCKETS.

3.3.2 Temperature calibration

A temperature calibration from 10°C to 40°C was done with concentrations of 1 M, 0.9 M and 0.8 M while measuring the intensity of the reflected light. This was done by making three small pouches with a fiber in the end as in the concentration calibration. In these pouches the short side across from the fiber will stay unseal while the rest of the sides of the pouch are sealed using a heat sealer (Magneta 421 MG). The pouches are then moved to the glovebox. First pouch is filled with 1 ml electrolyte (1M LiPF6 in EC:DMC (50:50)), second pouch is filled with 1 ml electrolyte and 0.111 ml DMC and third pouch is filled with 1 ml electrolyte and 0.250 ml DMC. This results in pouches with concentrations of 1 M, 0.9 M and 0.8 M. The pouches are then moved to a

temperature chamber where the set temperature is 10°C. After at least 2 hours and 45 minutes the temperature is increased by 10°C, which is repeated every 2 hours and 45 minutes until the temperature reaches 40°C. The single mode fiber was spliced to a pigtail fiber and connected to a fiber optic sensing interrogator (HYPERION si255 Fiber Optic Sensing Interrogator). The results were analyzed, stored and implemented in the same way for the three pouches as for the concentration calibration, with an addition of temperature being measured and stored every minute in a CSV file by the use of the Arbin LBT battery tester. The script can be found in the Appendix 7.2. The calibration was done twice.

3.4 Wetting and formation

The wetting and formation procedure was done according to "Fast formation cycling for lithium ion batteries" written by An et al. [50]. The first wetting is set for 2 hours. The wetting continues at 1.5 V for 4 hours to avoid corrosion of the copper collector. The battery is then rested for 12 hours before it is charged with a c-rate of C/10 until it reaches 3.9 V. The formation schedule is 5 cycles where the battery is rested at 3.9 V for 30 minutes before a C/10 charge to 4.2 V and a C/10 discharge to 3.9 V and rested again for 30 minutes. Lastly, the battery is charged with C/10 to 4.2 V, before resting at the upper voltage for an hour and then discharged at C/10 to 3 V. The schedule and an example of the voltage – time plot can be found in the Appendix 7.3.

3.5 Battery testing

3.5.1 Verification

A verification procedure was done before testing the batteries in order to evaluate if the battery or the sensor in the battery was useable for the cycling schedule and the measuring of reflected intensity. The procedure was done before and after the wetting and formation procedure. After the implementation of the optical fiber in the battery and the splicing of the single mode fiber to the pigtail fiber connected to the fiber optic sensing interrogator, the sensing analysis software Enlight was used to verify the sensors and batteries. The wanted result was a roughly straight line in the plot of the intensity (dBm) per wavelength (nm). However, often the result showed a clearly unilinear line, a dotted line or a line at -60 dBm, as this value is the lowest Enlight can measure. Actions as changing the angle of the fiber into the battery and pressing down on the middle of the battery were done to try to improve the result. As it was not certain if the problem was a broken fiber, gas in front of the fiber or if the electrolyte had not reached the fiber as the battery still needed to be wetted, the wetting and formation procedure was started before evaluating if the battery could be used. If the results had not been improved after the procedure, the battery was redeemed not useable for the further testing of the sensor.

3.5.2 Test with different C-rates

The sensor was tested through cycles of different c-rates of the battery, while the fiber was spliced and connected to a fiber optic sensing interrogator (HYPERION si255 Fiber Optic Sensing Interrogator). The schedule started with the battery being rested for 30 minutes. Before the testing with different c-rates, an initial CCCV

(constant current constant voltage) charge was done at 1 C until 4.2 V. Followed with a rest at upper voltage for 2 hours. Now the testing of different c-rates began. At each upper and lower voltage in the schedule, there was a 15 minute rest. Every charge was a CCCV, as it will then have the same starting point before discharging. Two cycles of C/20 were done, three C/10, five C/2, five 1 C, five 2 C and five 3 C. After the schedule was done, it started again with the C/20 cycles and was repeated until manually stopped. The full schedule can be found in the Appendix 7.4.

The test was analyzed, stored and implemented in the same way as the calibrations was. Several values measured by the Arbin LBT battery tester, as voltage, current and temperature, was stored each minute in a CSV file. 10000 points of intensity between wavelengths of 1500 nm and 1600 nm with a delta of 0.01 nm was stored every 2.5 minutes using ENLIGHT. The result was further implemented through a MATLAB script, where the average of all 10000 points per time was calculated, and a plot of intensity per time was made. The script can be found in the Appendix 7.4.

4 Results and Discussion

In this section the results from the concentration calibration, temperature calibration with different concentrations and the results from cycling the batteries with different c-rates are shown and discussed.

4.1 Concentration calibration

As explained in detail section 3.3.1, the concentration calibration will occur in room temperature with a fiber in a pouch filled with electrolyte (1 M $LiPF_6$ in EC:DMC (50:50)) and DMC. The concentration in the electrolyte measured will change from 1M to 0.9M, 0.8M and lastly 0.7M $LiPF_6$ by being diluted with DMC.

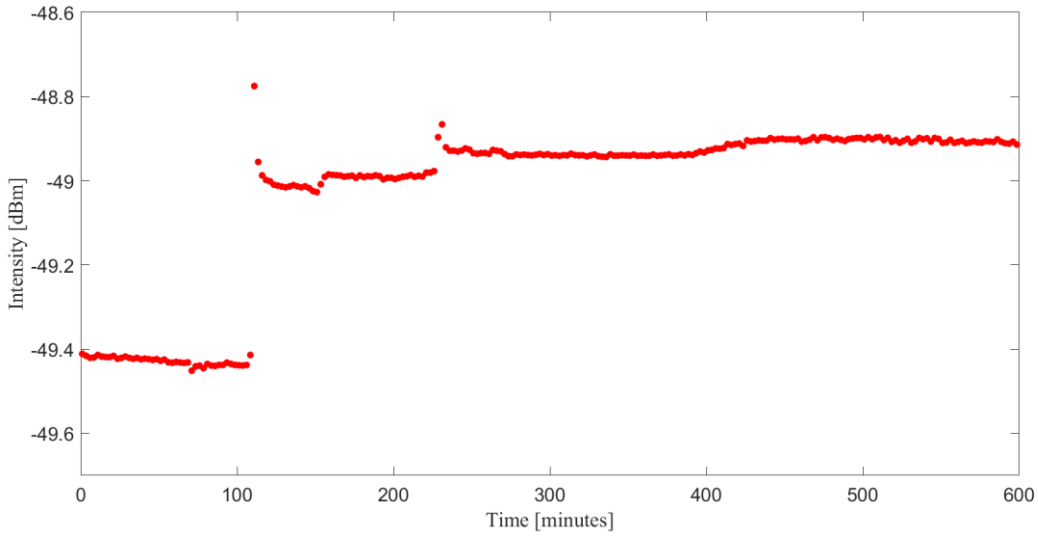

FIGURE 10: THE GRAPH SHOWS THE MEASURED INTENSITY IN THE ELECTROLYTE OUTSIDE OF THE FIBER DURING THE TIME WHEN THE ELECTROLYTE IS DILUTED FROM 1M TO 0.9M, 0.8M AND 0.7M. THE TIME INTERVAL BETWEEN EACH TIME THE ELECTROLYTE IS DILUTED IS TWO HOURS.

The graph shown in Figure 10 represents the measured intensity in the time period one of the two concentration calibration were conducted. The intensity is stable before each change in concentration, which happened each two hours, before the intensity quickly becomes stable again. From Figure 10 it is noticeable that the change in intensity between each change of concentration decreases as the electrolyte gets diluted towards 0.7M. The small change in intensity before 150 minutes is caused by readjusting the angle of the pouch. This indicates that the sensor is highly sensitive to changes in position. This can lead to many different results as it is hard to replicate the exact same position and angle of the fiber. During the changes in concentrations, the pouch was moved as a result of trying to mix the DMC with the electrolyte as gravity will not make the small volume of DMC flow down to the electrolyte, but rather stay as droplets on the wall inside the pouch. This uncertainty can result in the points being inaccurate and therefore the concentration calibration line to be inaccurate.

Two concentration calibrations were done. In Figure 11, a calibration line is plotted based on the line best fit according to the values presented. The values for each calibration were based on an average value from several values in the stable periods before changing the concentration. As shown in the graph, both calibrations were quite similar, with the exception of value at 0.9 M where difference being 0.402 dBm. The value at 0.9 M stands out even more as the only value where calibration 2 had a lower value compared to calibration 1 at the same concentration. The characteristic of the line in the figure is shown equation 3.

$$Intensity = (-2.4 \times value\ of\ the\ concentration) - 47.09 \quad (3)$$

Although previously discussed that the concentration calibration most likely is inaccurate from the results showed in Figure 10, the two concentration calibrations produced similar results with the exception of the values at 0.9 M. Arguable, one or both of the calibration had a pouch off-position as the result stood out from the rest.

Although the concentration calibration line is linear, it could make sense to have a small bend on the line as the Fresnel equation is a quadratic equation.

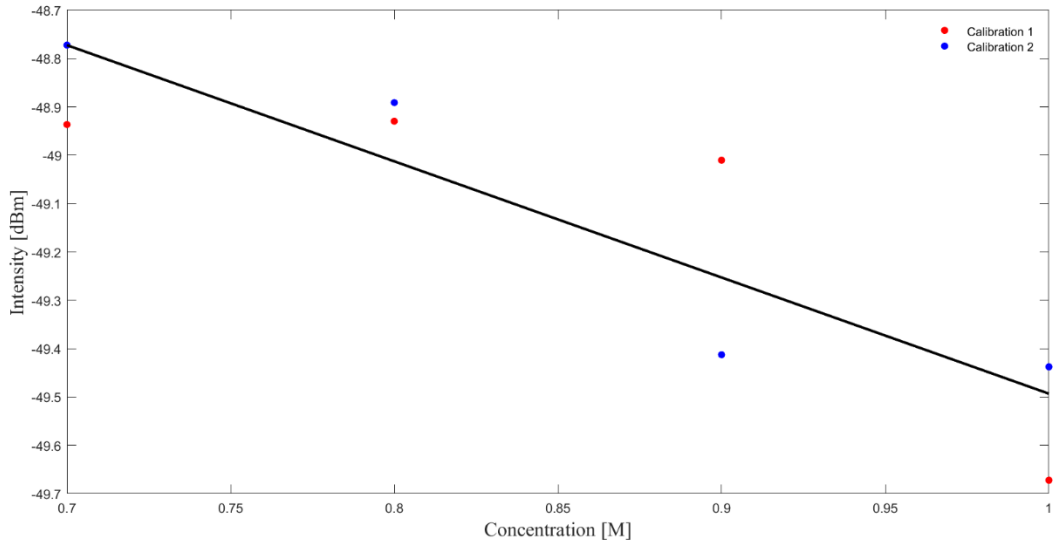

FIGURE 11: AN AVERAGE VALUE OF THE INTENSITY BEFORE EACH CHANGE IN CONCENTRATION FOR TWO DIFFERENT CONCENTRATION CALIBRATIONS. THE LINE REPRESENTS THE LINE OF BEST FIT FOR BOTH OF THE CALIBRATIONS.

4.2 Temperature calibration

The temperature calibration was as explained in 3.3.2 done with three different concentrations of electrolyte, where channel 5 had a concentration of 0.8M, channel 6 had a concentration of 0.9M and lastly channel 7 had a concentration of 1M $LiPF_6$. In Figure 12 the result of the temperature calibration is shown through a plot of the intensity over the duration of the calibration. Before the measurements of the intensity was started, the pouches with the different concentrations had already stayed in the temperature chamber for several hours at a

temperature of 10°C. From thereon the temperature was increased by 10°C every 2 hours and 45 minutes before reaching the final temperature of 40°C.

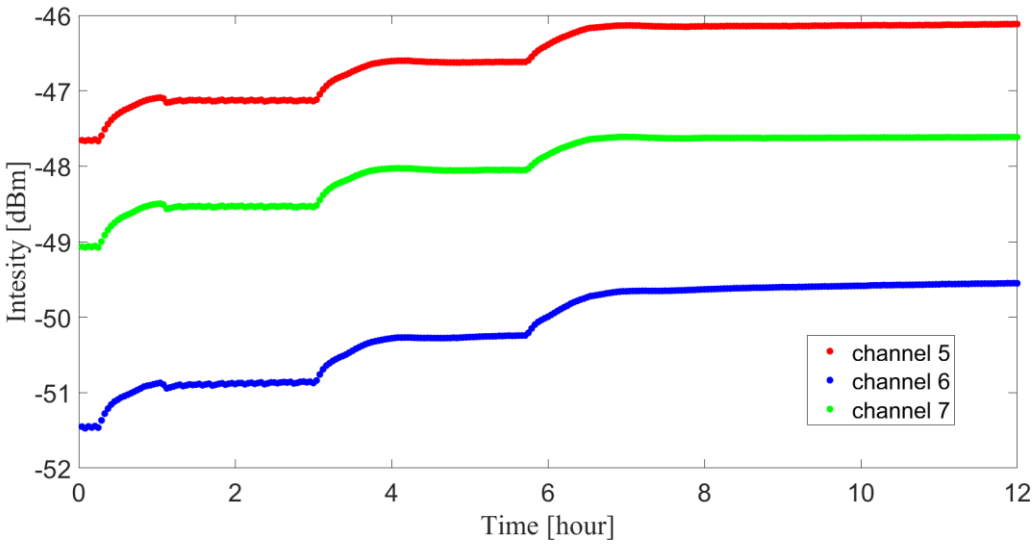

FIGURE 12: PLOT OF THE TEMPERATURE CALIBRATION OF THREE DIFFERENT VALUES OF CONCENTRATIONS. CHANNEL 5 HAD A CONCENTRATION OF 0.8M, CHANNEL 6 HAD 0.9M, WHILE CHANNEL 7 HAD 1M. THE TEMPERATURE WAS CHANGED FROM 10 DEGREES CELSIUS TO 40 DEGREES CELSIUS.

From Figure 12 it is observable that all of the sensors measured an approximately same change in intensity for each change in temperature. From the measured results the temperature chamber took around 30 minutes to increase 10 degrees Celsius, while the temperature and the sensor stabilized around 1 hour as observed in the graph. The experiment show that the values of the intensity from the sensor in the different electrolytes is quite spread and does not reflect on the difference in concentration, as the highest concentration is in the middle of the graphs. This furthermore indicated that the exact value of the intensity does not reflect on the concentration. The difference in the values may reflect on the angle and position of the fiber into the pouch, however when comparing the possible mistakes at the concentration calibration where the difference was 0.402 dBm, these differences are much bigger. The differences could reflect on the differences in the cut of the tip of the fiber from the cleaver. A small change in cut would affect the Fresnel equation and therefore the reflected light. However, as the different fibers will have the same cut throughout the experiments, the change in values is more interesting.

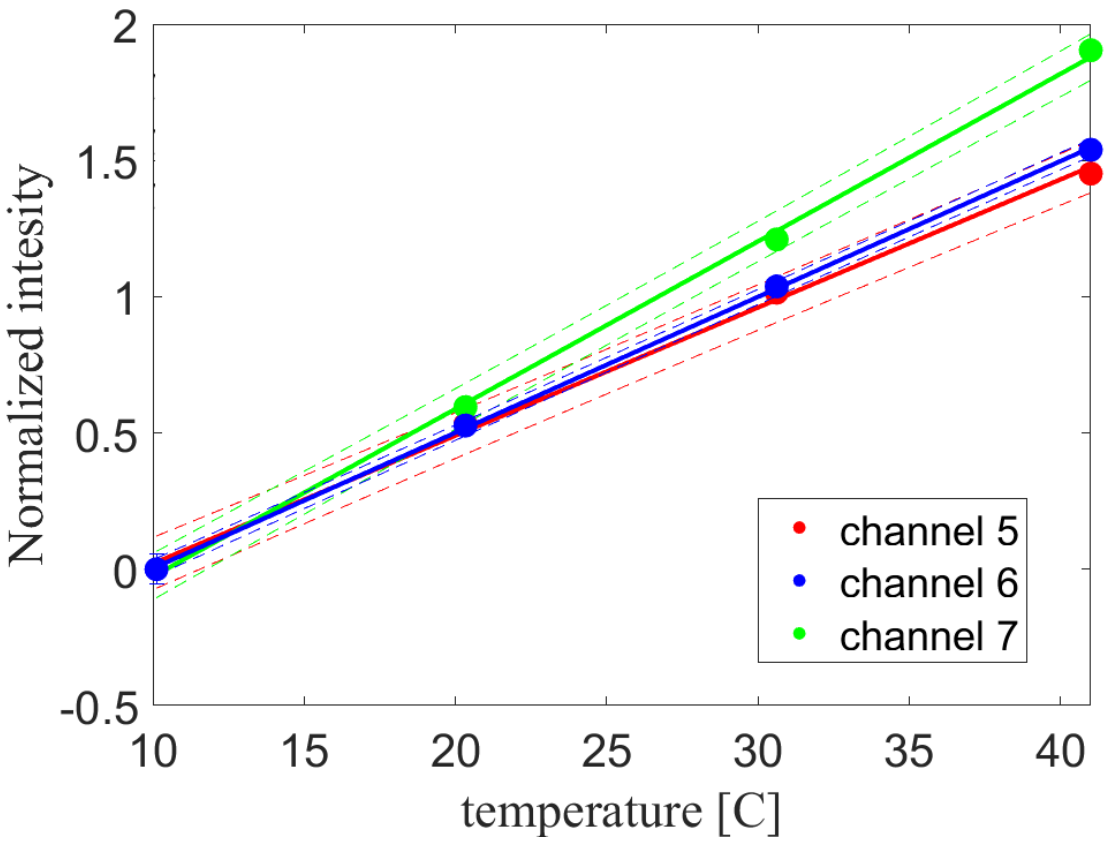

FIGURE 13: A TEMPERATURE CALIBRATION WITH DIFFERENT CONCENTRATIONS IN A PLOT WITH A NORMALIZED INTENSITY. CHANNEL 5 HAD A CONCENTRATION OF 0.8M, CHANNEL 6 HAD 0.9M, WHILE CHANNEL 7 HAD 1M. AN AVERAGE VALUE OF THE INTENSITY BEFORE EACH CHANGE IN TEMPERATURE FOR EACH CHANNEL. THE DOTTED LINES REPRESENT EACH CHANNELS ERROR.

The change in intensity as a temperature calibration line is shown in Figure 13. The plot chosen in a normalized intensity over the temperature change of the experiment as it can illustrate the difference in the channels in a better way. The points in the graph are taken from average of several points in the stable period before the change in temperature. The graph shows that the change in intensity during the calibration is fairly similar across the channels. Observably, channel 7 which has the highest concentration also has the steepest calibration line, and channel 5 which has the lowest concentration has the least increase in the calibration line of the three channels. However, the temperature calibration line of channel 5 and 6 is almost identical, as channel 6 falls into channel 5's error in the graph. For this experiment this could indicate that there is no difference in the temperature calibration line between 0.9 M and 0.8 M. Arguably, this could be interpreted as there being not a big difference in the temperature calibration line along different concentrations.

4.3 Battery testing

After the wetting and formation procedure described in 3.4, the batteries were cycled at different C-rates as the sensor was measuring the intensity from the reflected light. The result of four of these batteries will be shown

here. All the batteries were run through a schedule where they were initially charged with a 1C CCCV (constant current constant voltage) charge until it reached 100% SoC, before it cycled two C/20 cycles, three C/10 cycles, five C/2, five 1C, five 2C and five 3C cycles. Each cycle had a CCCV charge until the battery reached 100% SoC.

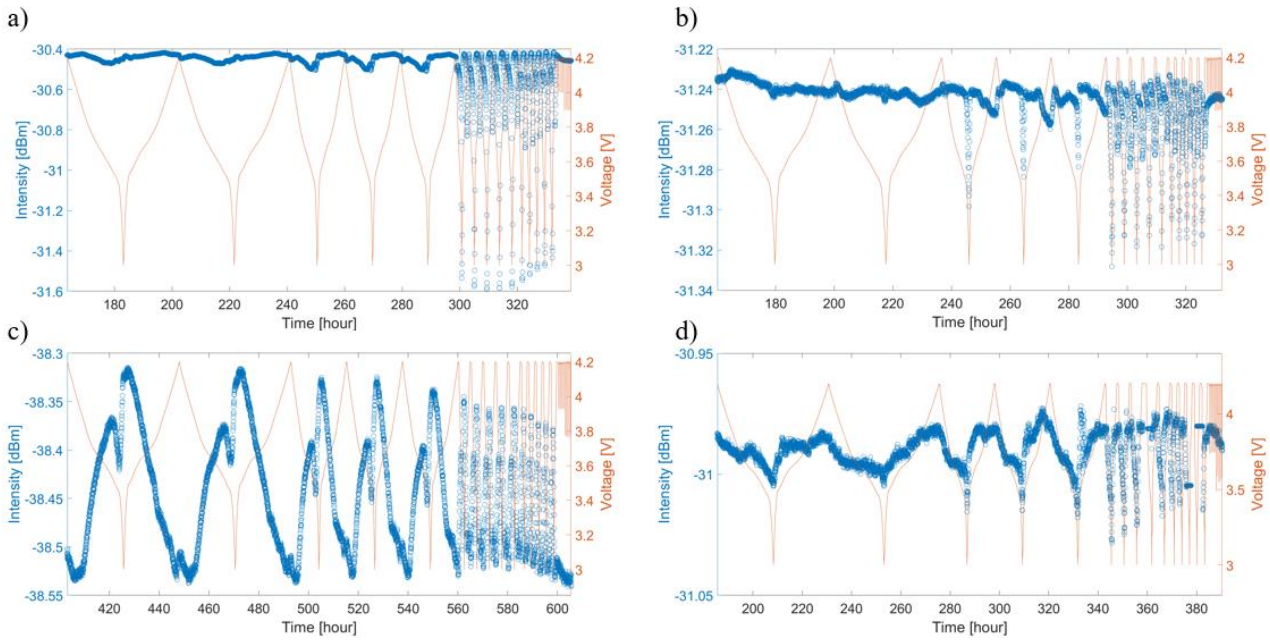

FIGURE 14: A FULL CYCLING SCHEDULE OF THE MEASURED REFLECTED INTENSITY DURING THE SCHEDULE. THE FIGURE SHOWS THE FULL SCHEDULE OF FOUR DIFFERENT BATTERIES. THEY ARE CYCLED THROUGH TWO C/20 CCCV CYCLES, THREE C/10 CCCV CYCLES, FIVE C/2, 1C, 2C AND 3C CCCV CYCLES.

From Figure 14 you can see all four batteries in a full cycling schedule. The plot shows the change in intensity during the schedule. The change in intensity is quite stable during the C/20 and C/10 cycles, before increasingly being more unstable from C/2 until 3C. This is more observable when looking at battery a) and battery b), where the sensor in battery a) varied between -30.4 dBm and -30.5 dBm at C/20 and C/10 before reaching values of -31.6 dBm in the cycles following.

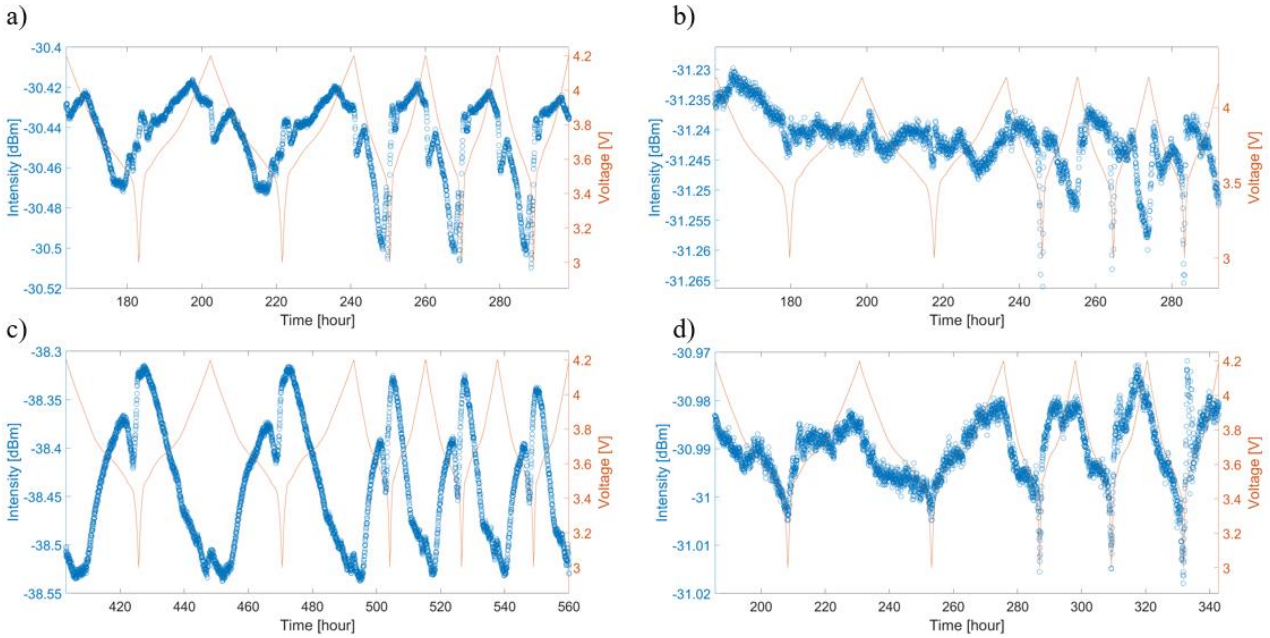

FIGURE 15: A CLOSEUP ON THE C/20 AND C/10 CYCLING OF THE MEASURED REFLECTED INTENSITY DURING THE SCHEDULE. THE FIGURE SHOWS THE CYCLING OF FOUR DIFFERENT BATTERIES. THEY ARE CYCLED THROUGH TWO C/20 CCCV CYCLES AND THREE C/10 CCCV CYCLES.

Therefore, it is more interesting to look at the results of the CCCV cycles at C/20 and C/10, as shown in Figure 15, as the changes in reflected intensity is more visible. From the plot it is obvious that the differences in the changes in the measured reflected intensity between charging and discharging the battery is big when comparing the different batteries. Battery c) has a ten times bigger difference in the highest measured intensity to the lowest measured intensity compared to battery b). Furthermore, battery c) shows peaks in intensity close to the 0% SoC of the battery, while the other batteries show peaks close to the 100% SoC. The difference in both magnitude but also position of peaks could be explained by the fiber not being exactly in the middle of the electrodes. As the positive lithium-ions migrate from one electrode to the other, the counterpart from the electrolyte, the anion PF_6^-, migrates to the other electrode, creating a concentration gradient between the electrodes. This could result in different intensity profiles during the voltage cycles depending on where the fiber in positioned in the concentration gradient.

As seen in battery c) there is a dip and then an increase at the 15 minutes rest at 100% DoD and a small increase at the 15 minutes rest at 100% SoC. Similar effects can be noticed in the plots of the other batteries. The increases in intensity could be explained by a higher temperature in the battery at 0% SoC, and we know from the temperature calibration at the intensity increases at an increase in temperature.

5 Conclusion and Future work

To get a better understanding of the state of health issue and life expectancy of a lithium-ion battery, measurements of the capacity and therefore the concentration of available lithium ions in the battery is valuable. A way of measuring the lithium-ion concentration while the battery is cycling can increase the overall knowledge of the change in capacity and help improve the battery longevity.

In this thesis four batteries were tested with an implemented optical fiber as a sensor to measure the intensity of the reflected light. Before the batteries was tested with different C-rates, the sensor was calibrated with regards for the change in concentration and the change in temperature. During the concentration calibrations it was noticed that a small change in position of the pouch and the angle of the fiber affected the intensity measurements of the fiber. However, several points in the two calibrations were similar, resulting in two similar concentration calibration lines. After the temperature calibration of three different concentrations, it was observed that the highest concentration was in between the two other concentrations in the intensity per time plot. Consequently, it was confirmed that the exact values of the intensity could vary, depending on variables like the position of the pouch, angle of the fiber, cut of the top of the fiber or other variables. Therefore, the change in intensity was more interesting than the exact value. When evaluating the temperature calibration lines, it was observed that the change in temperature is quite similar across the different concentrations. Which can be interpreted as there not being a big difference in the change in temperature depending on the concentration.

After the calibrations tests of different C-rates was conducted on batteries with optical fibers implemented. Results showed a visible pattern of the measured reflected intensity for C/20 and C/10, however the results were more chaotic at C/2 and 1 C and not visible at c-rates above. Even though the results showed pattern, the different intensity per voltage cycle varied in magnitude and placements of peaks during the cycle. This can arguably be explained by the position of the optical fiber between the electrodes compared to the concentration gradients created by migration of ions and anions. Furthermore, there was an increase in the intensity at rest at 0% SoC and 100% SoC. The increase at 0% SoC could be explained by the increase in temperature.

In summary, the results show that measurements of reflected intensity and concentration can vary depending on several variables, but that a SoC-dependent pattern forms during the cycle. This is important because it shows that the sensor is working and can be used to better understand the change in concentration and capacity.

Further work can include several optical fibers implemented in the same battery during testing. Either at different placements, or more interesting between the same electrode but with separators in between them to observe if the position of the fiber between the electrodes makes a difference in the result. To ensure more accurate calibrations and more accurate testing new methods should be tried.

6 References

[1] A. G. Olabi and M. A. Abdelkareem, “Renewable energy and climate change,” *Renewable and Sustainable Energy Reviews*, vol. 158, Apr. 2022, doi: 10.1016/j.rser.2022.112111.

[2] D. Gielen, F. Boshell, D. Saygin, M. D. Bazilian, N. Wagner, and R. Gorini, “The role of renewable energy in the global energy transformation,” *Energy Strategy Reviews*, vol. 24, pp. 38–50, Apr. 2019, doi: 10.1016/j.esr.2019.01.006.

[3] D. Maradin, “Advantages and disadvantages of renewable energy sources utilization,” *International Journal of Energy Economics and Policy*, vol. 11, no. 3, pp. 176–183, 2021, doi: 10.32479/ijeep.11027.

[4] T. Chen *et al.*, “Applications of Lithium-Ion Batteries in Grid-Scale Energy Storage Systems,” *Transactions of Tianjin University*, vol. 26, no. 3. Tianjin University, pp. 208–217, Jun. 01, 2020. doi: 10.1007/s12209-020-00236-w.

[5] W. Liu, T. Placke, and K. T. Chau, “Overview of batteries and battery management for electric vehicles,” *Energy Reports*, vol. 8. Elsevier Ltd, pp. 4058–4084, Nov. 01, 2022. doi: 10.1016/j.egyr.2022.03.016.

[6] M. Li, J. Lu, Z. Chen, and K. Amine, “30 Years of Lithium-Ion Batteries,” *Advanced Materials*, vol. 30, no. 33. Wiley-VCH Verlag, Aug. 16, 2018. doi: 10.1002/adma.201800561.

[7] N. A. Padilla *et al.*, “Tracking lithium ions via widefield fluorescence microscopy for battery diagnostics,” *ACS Sens*, vol. 2, no. 7, pp. 903–908, Jul. 2017, doi: 10.1021/acssensors.7b00087.

[8] A. Nedjalkov *et al.*, “Refractive Index Measurement of Lithium Ion Battery Electrolyte with Etched Surface Cladding Waveguide Bragg Gratings and Cell Electrode State Monitoring by Optical Strain Sensors,” *Batteries*, vol. 5, no. 1, p. 30, Mar. 2019, doi: 10.3390/batteries5010030.

[9] J. Huang *et al.*, “Monitoring battery electrolyte chemistry: Via in-operando tilted fiber Bragg grating sensors,” *Energy Environ Sci*, vol. 14, no. 12, pp. 6464–6475, Dec. 2021, doi: 10.1039/d1ee02186a.

[10] J. J. Lamb and B. Pollett, “Micro-Optics and Energy Sensors forrEnergy Devices.”

[11] O. S. Burheim, “Secondary Batteries,” in *Engineering Energy Storage*, Elsevier, 2017, pp. 111–145. doi: 10.1016/B978-0-12-814100-7.00007-9.

[12] D. Stanulewicz *et al.*, “EDITOR-IN-CHIEF COVER DESIGN”, [Online]. Available: http://cejsh.icm.edu.pl

[13] J. J. L. 1&2, B. G. Pollet, O. S. Burheim, T. E. Jensen, and K. Johansson, “FEASIBILITY STUDY REPORT Establishing Giga Factories for Manufacturing of Li-ion Batteries in Norway KIC InnoEnergy SE Innovation

Project Expanding and Accelerating Battery Cell Supply from Green, Ultra-Low Cost Production in the Nordic Region."

[14] X. Feng, M. Ouyang, X. Liu, L. Lu, Y. Xia, and X. He, "Thermal runaway mechanism of lithium ion battery for electric vehicles: A review," *Energy Storage Materials*, vol. 10. Elsevier B.V., pp. 246–267, Jan. 01, 2018. doi: 10.1016/j.ensm.2017.05.013.

[15] "A General Discussion of Li Ion Battery Safety."

[16] M. Gu *et al.*, "Formation of the spinel phase in the layered composite cathode used in Li-Ion batteries," *ACS Nano*, vol. 7, no. 1, pp. 760–767, Jan. 2013, doi: 10.1021/nn305065u.

[17] T. Kakuda, K. Uematsu, K. Toda, and M. Sato, "Electrochemical performance of Al-doped LiMn2O4 prepared by different methods in solid-state reaction," *J Power Sources*, vol. 167, no. 2, pp. 499–503, May 2007, doi: 10.1016/J.JPOWSOUR.2007.01.035.

[18] G. Luo *et al.*, "Electrochemical recovery lithium from brine via taming surface wettability of regeneration spent batteries cathode materials," *Appl Energy*, vol. 337, p. 120890, May 2023, doi: 10.1016/J.APENERGY.2023.120890.

[19] H. Walvekar, H. Beltran, S. Sripad, and M. Pecht, "Implications of the Electric Vehicle Manufacturers' Decision to Mass Adopt Lithium-Iron Phosphate Batteries," *IEEE Access*, vol. 10, pp. 63834–63843, 2022, doi: 10.1109/ACCESS.2022.3182726.

[20] C. H. Chen, J. Liu, M. E. Stoll, G. Henriksen, D. R. Vissers, and K. Amine, "Aluminum-doped lithium nickel cobalt oxide electrodes for high-power lithium-ion batteries," *J Power Sources*, vol. 128, no. 2, pp. 278–285, Apr. 2004, doi: 10.1016/J.JPOWSOUR.2003.10.009.

[21] N. Yabuuchi and T. Ohzuku, "Novel lithium insertion material of LiCo1/3Ni1/3Mn1/3O2 for advanced lithium-ion batteries," *J Power Sources*, vol. 119–121, pp. 171–174, Jun. 2003, doi: 10.1016/S0378-7753(03)00173-3.

[22] M. Wissler, "Graphite and carbon powders for electrochemical applications," *Journal of Power Sources*, vol. 156, no. 2. pp. 142–150, Jun. 01, 2006. doi: 10.1016/j.jpowsour.2006.02.064.

[23] G. Sun, S. Bhattacharya, and A. T. Alpas, "Cyclic strain-induced crack growth in graphite during electrochemical testing in propylene carbonate-based Li-ion battery electrolytes," *J Mater Sci*, vol. 53, no. 2, pp. 1297–1309, Jan. 2018, doi: 10.1007/s10853-017-1547-y.

[24] N. A. Kaskhedikar and J. Maier, “Lithium Storage in Carbon Nanostructures”, doi: 10.1002/adma.200901079.

[25] P. Porion, Y. R. Dougassa, C. Tessier, L. El Ouatani, J. Jacquemin, and M. Anouti, “Comparative study on transport properties for LiFAP and LiPF6 in alkyl-carbonates as electrolytes through conductivity, viscosity and NMR self-diffusion measurements,” *Electrochim Acta*, vol. 114, pp. 95–104, 2013, doi: 10.1016/j.electacta.2013.10.015.

[26] V. Aravindan, J. Gnanaraj, S. Madhavi, and H. K. Liu, “Lithium-ion conducting electrolyte salts for lithium batteries,” *Chemistry - A European Journal*, vol. 17, no. 51. pp. 14326–14346, Dec. 16, 2011. doi: 10.1002/chem.201101486.

[27] S. S. Zhang, “A review on the separators of liquid electrolyte Li-ion batteries,” *Journal of Power Sources*, vol. 164, no. 1. pp. 351–364, Jan. 10, 2007. doi: 10.1016/j.jpowsour.2006.10.065.

[28] G. Seo *et al.*, “Rapid determination of lithium-ion battery degradation: High C-rate LAM and calculated limiting LLI,” *Journal of Energy Chemistry*, vol. 67, pp. 663–671, Apr. 2022, doi: 10.1016/j.jechem.2021.11.009.

[29] Q. Liu *et al.*, “Understanding undesirable anode lithium plating issues in lithium-ion batteries,” *RSC Adv*, vol. 6, no. 91, pp. 88683–88700, 2016, doi: 10.1039/c6ra19482f.

[30] N. Nitta, F. Wu, J. T. Lee, and G. Yushin, “Li-ion battery materials: Present and future,” *Materials Today*, vol. 18, no. 5. Elsevier B.V., pp. 252–264, Jun. 01, 2015. doi: 10.1016/j.mattod.2014.10.040.

[31] A. Banerjee, B. Ziv, Y. Shilina, S. Luski, I. C. Halalay, and D. Aurbach, “Multifunctional Manganese Ions Trapping and Hydrofluoric Acid Scavenging Separator for Lithium Ion Batteries Based on Poly(ethylene-alternate-maleic acid) Dilithium Salt,” *Adv Energy Mater*, vol. 7, no. 3, Feb. 2017, doi: 10.1002/aenm.201601556.

[32] D. Aurbach *et al.*, “Review on electrode-electrolyte solution interactions, related to cathode materials for Li-ion batteries,” *Journal of Power Sources*, vol. 165, no. 2. pp. 491–499, Mar. 20, 2007. doi: 10.1016/j.jpowsour.2006.10.025.

[33] M. Broussely *et al.*, “Main aging mechanisms in Li ion batteries,” in *Journal of Power Sources*, Aug. 2005, pp. 90–96. doi: 10.1016/j.jpowsour.2005.03.172.

[34] Y. nan Zhang, Y. Sun, L. Cai, Y. Gao, and Y. Cai, “Optical fiber sensors for measurement of heavy metal ion concentration: A review,” *Measurement: Journal of the International Measurement Confederation*, vol. 158. Elsevier B.V., Jul. 01, 2020. doi: 10.1016/j.measurement.2020.107742.

[35] D. C. Abeysinghe, S. Dasgupta, J. T. Boyd, and H. E. Jackson, “A Novel MEMS Pressure Sensor Fabricated on an Optical Fiber,” 2001.

[36] P. Roriz, S. Silva, O. Frazão, and S. Novais, “Optical fiber temperature sensors and their biomedical applications,” *Sensors (Switzerland)*, vol. 20, no. 7. MDPI AG, Apr. 01, 2020. doi: 10.3390/s20072113.

[37] S. Ma *et al.*, “Optical Fiber Sensors for High-Temperature Monitoring: A Review,” *Sensors*, vol. 22, no. 15. MDPI, Aug. 01, 2022. doi: 10.3390/s22155722.

[38] J. Li, “A review: Development of novel fiber-optic platforms for bulk and surface refractive index sensing applications,” *Sensors and Actuators Reports*, vol. 2, no. 1. Elsevier B.V., Nov. 01, 2020. doi: 10.1016/j.snr.2020.100018.

[39] S. C. Her and C. M. Yang, “Dynamic strain measured by mach-zehnder interferometric optical fiber sensors,” *Sensors*, vol. 12, no. 3, pp. 3314–3326, Mar. 2012, doi: 10.3390/s120303314.

[40] X. Bao and L. Chen, “Recent Progress in Distributed Fiber Optic Sensors,” *Sensors (Switzerland)*, vol. 12, no. 7. pp. 8601–8639, Jul. 2012. doi: 10.3390/s120708601.

[41] Y. J. Rao, “Recent progress in applications of in-"bre Bragg grating sensors,” 1999.

[42] B. H. Lee *et al.*, “Interferometric fiber optic sensors,” *Sensors*, vol. 12, no. 3. pp. 2467–2486, Mar. 2012. doi: 10.3390/s120302467.

[43] N. Shabairou, B. Lengenfelder, M. Hohmann, F. Klämpfl, M. Schmidt, and Z. Zalevsky, “All-optical, an ultra-thin endoscopic photoacoustic sensor using multi-mode fiber,” *Sci Rep*, vol. 10, no. 1, Dec. 2020, doi: 10.1038/s41598-020-66076-9.

[44] B. E. A. Saleh and M. Carl. Teich, *Fundamentals of photonics*. Wiley, 1991.

[45] X. Lu, P. J. Thomas, and J. O. Hellevang, “A Review of Methods for Fibre-Optic Distributed Chemical Sensing”, doi: 10.3390/s19132876.

[46] J. J. Davenport, M. Hickey, J. P. Phillips, and P. A. Kyriacou, “Fiber-optic fluorescence-quenching oxygen partial pressure sensor using platinum octaethylporphyrin,” *Appl Opt*, vol. 55, no. 21, p. 5603, Jul. 2016, doi: 10.1364/ao.55.005603.

[47] C. Gervillié-Mouravieff, L. Albero Blanquer, C. Alphen, J. Huang, and J. M. Tarascon, “Unraveling SEI formation and cycling behavior of commercial Ni-rich NMC Li-ion pouch cells through operando optical characterization,” *J Power Sources*, vol. 580, p. 233268, Oct. 2023, doi: 10.1016/J.JPOWSOUR.2023.233268.

[48] A. K. Stephan, “A Pathway to Understand NMC Cathodes,” *Joule*, vol. 4, no. 8, pp. 1632–1633, Aug. 2020, doi: 10.1016/J.JOULE.2020.08.004.

[49] “Light,” *Plant Factory: An Indoor Vertical Farming System for Efficient Quality Food Production*, pp. 115–128, Jan. 2016, doi: 10.1016/B978-0-12-801775-3.00007-X.

[50] S. J. An, J. Li, Z. Du, C. Daniel, and D. L. Wood, “Fast formation cycling for lithium ion batteries,” *J Power Sources*, vol. 342, pp. 846–852, Feb. 2017, doi: 10.1016/J.JPOWSOUR.2017.01.011.

[51] M. Åtland, “In operando measurements of the lithium-ion concentration in lithium-ion batteries,” unpublished, April. 2022.

[52] M. S. Wahl et al., “Fiber-optic lithium sensing in lithium-ion batteries”, unpublished, 2023.

[53] “What is an optical fiber?”, Smartoptics. Available: https://smartoptics.com/knowledgebank-post/what-is-an-optical-fiber/ [Accessed: June 22, 2023]

[54] M. S. Wahl, “Optical sensing in batteries_MSW”, Institutt for energi- og prosessteknikk, NTNU, 2021.

7 Appendices

7.1 Concentration calibration

```
close all
clear all
clc
SIZE =5;
FT=15;

files = dir('D:\Master\19_04_23_Magnus_Third_Concentration_Calibration\Magnus_third_concentration_calibration_19_04_23_(port_2)\2023\04\data_full_experiment.txt');

data_all = importdata(files.name);
name = files.name;
data_temp = data_all(:,1);

time = 1:2.5:length(data_temp)*2.5;
index = 1:length(data_temp);

figure(1011)
plot(index,data_temp,'ro','MarkerFaceColor','r','MarkerSize',SIZE)

h4 = figure(100)
plot(time,data_temp,'ro','MarkerFaceColor','r','MarkerSize',SIZE)
% hold on
% plot(wavelenght,channel_6_data,'bo-','MarkerFaceColor','b','MarkerSize',SIZE)


FT = 15;
ylabel ('Intensity [dBm]',  'FontSize', FT, 'FontName', 'Times')
xlabel ('Time [minutes]',  'FontSize', FT, 'FontName', 'Times')

set(gca,'FontSize',15)
axis([0 600 -49.7 -48.6])

% legend('channel 5','channel 6','Location','southeast')
% title('1 measurement')


% dat = [time' data_temp];
% dat1 = [normalized_time' dataofinterest2'];
% dat2 = normalized_time(images(mm));
% writematrix(dat ,'data_full_temp', "FileType","text");

% exportgraphics(h4,['temp_' name '.png'])

%% average and error

before_changing_temperatura_index = [30 78 126 174];
points_evaluated = 4;
Temp_ = [];
% xaxis= [1 0.9 0.8 0.7];
% xaxis= [1 2 3 4];

for i =1:length(before_changing_temperatura_index)
initial = before_changing_temperatura_index(i) - points_evaluated;
end_point = before_changing_temperatura_index(i);
    Temp_ = data_temp(initial:end_point);

    Mean(i) = mean(Temp_);
    error(i) = std(Temp_);

end

figure(2011)
plot(index,data_temp,'ro','MarkerFaceColor','r','MarkerSize',SIZE)
errorbar(Mean,error,'ro','MarkerFaceColor','r','MarkerSize',SIZE)
ylabel ('Intensity',  'FontSize', FT, 'FontName', 'Times')
xlabel ('index',  'FontSize', FT, 'FontName', 'Times')

set(gca,'FontSize',20)

% legend('channel 5','channel 6','Location','southeast')
title('Concentration calibration line')
hold on
```

FIGURE 16: PART 1 OF THE CODE FOR THE PLOTS USED IN THE RESULTS.

```
 dat = [Mean' error'];
% dat1 = [normalized_time' dataofinterest2'];
% dat2 = normalized_time(images(mm));
writematrix(dat ,'mean_error_channel2', "FileType","text");

%Plotting the line of best fit
% concentration = [1 0.9 0.8 0.7];
concentration = [1 2 3 4];
Points = [-49.4376 -48.9903 -48.9389 -48.9076];

p=polyfit(concentration,Points,1);
x1=linspace(min(concentration), max(concentration), 100);
y1=polyval(p,x1);
plot(x1,y1,'k-', 'LineWidth',2);
X_int = roots (p);
y_int = p(2);
eq_str = sprintf('y = %.2fx + %.2f', p);
text(min(concentration)+0.02, max(Points)-0.01, eq_str, ... % An example of setting the position
    'FontSize', 16)
%%
SIZE =5;
points1=[-49.6721 -49.0103 -48.9296 -48.9365];
points2=[-49.4376 -49.41258 -48.891117 -48.7722];
xaxis=[1 0.9 0.8 0.7];

figure(3011)
plot(xaxis,points1,'ro','MarkerFaceColor','r','MarkerSize',SIZE)
% errorbar(Mean,error,'ro','MarkerFaceColor','r','MarkerSize',SIZE)
ylabel ('Intensity [dBm]',  'FontSize', FT, 'FontName', 'Times')
xlabel ('Concentration [M]',  'FontSize', FT, 'FontName', 'Times')

hold on

plot(xaxis,points2,'bo','MarkerFaceColor','b','MarkerSize',SIZE)
% errorbar(Mean,error,'ro','MarkerFaceColor','r','MarkerSize',SIZE)
ylabel ('Intensity [dBm]',  'FontSize', FT, 'FontName', 'Times')
xlabel ('Concentration [M]',  'FontSize', FT, 'FontName', 'Times')

axis([0.7 1 -49.7 -48.7]);

legend('Calibration 1','Calibration 2');%,'Location','northwest')

set(legend, 'Box', 'off');

concentration = [1 0.9 0.8 0.7];
Points = (points1+points2)/2;

p=polyfit(concentration,Points,1);
x1=linspace(min(concentration), max(concentration), 100);
y1=polyval(p,x1);
plot(x1,y1,'k-', 'LineWidth',2);
X_int = roots (p);
y_int = p(2);
eq_str = sprintf('y = %.2fx + %.2f', p);
% text(min(concentration)+0.02, max(Points)-0.01, eq_str, ... % An example of setting the position
%     'FontSize', 16)
```

FIGURE 17: PART 2 OF THE CODE FOR THE PLOTS USED IN THE RESULTS.

7.2 Temperature calibration

```
close all
clear all
clc

files = dir('D:\Magnus_second_concentration_calibration_(port_2)_and_third_temp_calibration_(port_5,6_and_7)(26.03)\Micron_optics_ENLIGHT\03\Responses*.txt');

% only first file
for jj = 1
numlines = 10000;
k = 114;
for i=1:46

m = i-1;
aa= k+18*m;
fileID = fopen(files(jj).name);
thissectionCell = textscan(fileID, '%f', numlines, 'HeaderLines', aa, 'CollectOutput', 1);
data = cell2mat(thissectionCell);
data_mean_channel_5(i) = mean(data);
thissectionCell = textscan(fileID, '%f', numlines, 'HeaderLines', 1, 'CollectOutput', 1);
data = cell2mat(thissectionCell);
data_mean_channel_6(i) = mean(data);
thissectionCell = textscan(fileID, '%f', numlines, 'HeaderLines', 1, 'CollectOutput', 1);
data = cell2mat(thissectionCell);
data_mean_channel_7(i) = mean(data);

end
% time = 1:length(data_mean_channel_5);
% plot(time,data_mean_channel_5,'o')

end

dat = [data_mean_channel_5' data_mean_channel_6' data_mean_channel_7'];
% dat1 = [normalized_time' dataofinterest2'];
% dat2 = normalized_time(images(mm));
writematrix(dat ,['data_' num2str(jj)], "FileType","text");
% writematrix(dat1 ,['time_conectivity' namename], "FileType","text");
%%

close all
clear all
clc

files = dir('D:\Magnus_second_concentration_calibration_(port_2)_and_third_temp_calibration_(port_5,6_and_7)(26.03)\Micron_optics_ENLIGHT\03\Responses*.txt');

for jj = 7%:length(files)-1

 numlines = 10000;
% time = 0:10:

k = 5;
for i=1:46
m = i-1;
aa= k+18*m;
fileID = fopen(files(jj).name);
thissectionCell = textscan(fileID, '%f', numlines, 'HeaderLines', aa, 'CollectOutput', 1);
data = cell2mat(thissectionCell);
data_mean_channel_5(i) = mean(data);%(i+46*(jj-1))
thissectionCell = textscan(fileID, '%f', numlines, 'HeaderLines', 1, 'CollectOutput', 1);
data = cell2mat(thissectionCell);
data_mean_channel_6(i) = mean(data);
thissectionCell = textscan(fileID, '%f', numlines, 'HeaderLines', 1, 'CollectOutput', 1);
data = cell2mat(thissectionCell);
data_mean_channel_7(i) = mean(data);

end

end

% time = 1:length(data_mean_channel_5);
% plot(time,data_mean_channel_5,'o')

dat = [data_mean_channel_5' data_mean_channel_6' data_mean_channel_7'];
% dat1 = [normalized_time' dataofinterest2'];
% dat2 = normalized_time(images(mm));
```

FIGURE 18: PART 1 OF THE DATA PROCESSING AND SCRIPTS FOR THE PLOTS USED IN THE RESULTS OF THE TEMPERATURE CALIBRATION.

```
writematrix(dat ,['data_' num2str(jj)], "FileType","text");
% writematrix(dat1 ,['time_conectivity' namename], "FileType","text");

%%

close all
clear all
clc

figure(1)
SIZE = 5;
files = dir('D:\Magnus_second_concentration_calibration_(port_2)_and_third_temp_calibration_(port_5,6_and_7)(26.03)\Micron_optics_ENLIGHT\03\data*.txt');
data_to_plot = [];
data_to_plot_1 = [];
data_to_plot_2 = [];
for i=1:length(files)

final_data = importdata(files(i).name);

channel_5 = (final_data(:,1));
channel_6 = (final_data(:,2));
channel_7 = (final_data(:,3));
data_to_plot=cat(1,data_to_plot,channel_5);
data_to_plot_1=cat(1,data_to_plot_1,channel_6);
data_to_plot_2=cat(1,data_to_plot_2,channel_7);
% data_to_plot = [data_to_plot channel_5];
end
time = 1:length(data_to_plot);
real_time = (time*10)/60;
mm = 1;
plot(real_time(1:mm:end),data_to_plot(1:mm:end),'ro','MarkerFaceColor','r','MarkerSize',SIZE)
hold on
plot(real_time(1:mm:end),data_to_plot_1(1:mm:end),'bo','MarkerFaceColor','b','MarkerSize',SIZE)
plot(real_time(1:mm:end),data_to_plot_2(1:mm:end),'go','MarkerFaceColor','g','MarkerSize',SIZE)


FT = 15;
ylabel ('Intesity [XXX]',  'FontSize', FT, 'FontName', 'Times')
xlabel ('Time [min]',  'FontSize', FT, 'FontName', 'Times')

% axis ([0 1200 0 100])
set(gca,'FontSize',20)

legend('channel 5','channel 6')%,'Location','northwest')
title('Exp1')

%% Write text file of all data

dat = [data_to_plot data_to_plot_1 data_to_plot_2];
% dat1 = [normalized_time' dataofinterest2'];
% dat2 = normalized_time(images(mm));
writematrix(dat ,'data_full_experiment', "FileType","text");

%% FULL plot
figure(20)
clf
final_data_full = importdata('data_full_experiment.txt');
channel_5 = (final_data_full(:,1))';
channel_6 = (final_data_full(:,2))';
channel_7 = (final_data_full(:,3))';
mm =1;
SIZE = 5;
time = 1:length(channel_5);
real_time = (time*2.5)/60;

plot(real_time(1:mm:end),channel_5(1:mm:end),'ro','MarkerFaceColor','r','MarkerSize',SIZE)
hold on
plot(real_time(1:mm:end),channel_6(1:mm:end),'bo','MarkerFaceColor','b','MarkerSize',SIZE)
```

FIGURE 19: PART 2 OF THE DATA PROCESSING AND SCRIPTS FOR THE PLOTS USED IN THE RESULTS OF THE TEMPERATURE CALIBRATION.

```
plot(real_time(1:mm:end),channel_7(1:mm:end),'go','MarkerFaceColor','g','MarkerSize',SIZE)


FT = 15;
ylabel ('Intesity [dBm]',  'FontSize', FT, 'FontName', 'Times')
xlabel ('Time [hour]',  'FontSize', FT, 'FontName', 'Times')

% axis ([0 1200 0 100])
set(gca,'FontSize',20)

legend('channel 5','channel 6','channel 7')%,'Location','northwest')
% title('Exp2')



%% Plot calibration curve
close all
clear all
clc
SIZE =10;
FT=15;
figure (99)
concentration = [1 2 3 4 5];
channel_5_signal = [-46.8317 -46.8372 -46.8277 -46.827 -46.8315];
channel_6_signal = [-49.0734 -49.0026 -48.9729 -48.7997 -48.5038];
channel_7_signal = [-49.0734 -49.0026 -48.9729 -48.7997 -48.5038];




plot(concentration,channel_5_signal,'ro','MarkerFaceColor','r','MarkerSize',SIZE)
hold on
plot(concentration,channel_6_signal,'bo','MarkerFaceColor','b','MarkerSize',SIZE)
ylabel ('Intesity [dBm]',  'FontSize', FT, 'FontName', 'Times')
xlabel ('temperature [C]',  'FontSize', FT, 'FontName', 'Times')
set(gca,'FontSize',15)
% xlim([0 max(time_temp)])
legend('channel 5','channel 6','Location','southeast')
title('concentration calibration curve',  'FontSize', FT+5, 'FontName', 'Times')

%Plotting the line of best fit
p=polyfit(concentration,channel_5_signal,1);
x1=linspace(min(concentration), max(concentration), 100);
y1=polyval(p,x1);
plot(x1,y1,'k-', 'LineWidth',2);
X_int = roots (p);
y_int = p(2);
eq_str = sprintf('y = %.2fx + %.2f', p);
text(min(concentration)+0.02, max(channel_5_signal)-0.01, eq_str, ... % An example of setting the position
    'FontSize', 16)

%Plotting the line of best fit
p=polyfit(concentration,channel_6_signal,1);
x1=linspace(min(concentration), max(concentration), 100);
y1=polyval(p,x1);
plot(x1,y1,'k-', 'LineWidth',2);
X_int = roots (p);
y_int = p(2);
eq_str = sprintf('y = %.2fx + %.2f', p);
text(min(concentration)+0.02, max(channel_6_signal)-0.01, eq_str, ... % An example of setting the position
    'FontSize', 16)
```

FIGURE 20: PART 3 OF THE DATA PROCESSING AND SCRIPTS FOR THE PLOTS USED IN THE RESULTS OF THE TEMPERATURE CALIBRATION.

```
close all
clear all
clc
SIZE =10;
FT=15;

files = dir('D:\Master\Magnus_second_concentration_calibration_(port_2)_and_third_temp_calibration_(port_5,6_and_7)(26.03)\data_full_experiment_changed_concentration.txt');

data_all = importdata(files.name);
name = files.name;
data_temp = data_all(:,1);

time = 1:2.5:length(data_temp)*2.5;
index = 1:length(data_temp);

figure(1011)
plot(index,data_temp,'ro','MarkerFaceColor','r','MarkerSize',SIZE)

h4 = figure(100)
plot(time,data_temp,'ro','MarkerFaceColor','r','MarkerSize',SIZE)
% hold on
% plot(wavelenght,channel_6_data,'bo-','MarkerFaceColor','b','MarkerSize',SIZE)


FT = 15;
ylabel ('Temperature [C]',  'FontSize', FT, 'FontName', 'Times')
xlabel ('Time [minutes]',  'FontSize', FT, 'FontName', 'Times')

set(gca,'FontSize',20)

% legend('channel 5','channel 6','Location','southeast')
title('1 measurement')


% dat = [time' data_temp];
% dat1 = [normalized_time' dataofinterest2'];
% dat2 = normalized_time(images(mm));
% writematrix(dat ,'data_full_temp', "FileType","text");

% exportgraphics(h4,['temp_' name '.png'])

%% average and error

before_changing_temperatura_index = [5 53 102 288];
points_evaluated = 4;

for i =1:length(before_changing_temperatura_index)
initial = before_changing_temperatura_index(i) - points_evaluated;
end_point = before_changing_temperatura_index(i);
    Temp_ = data_temp(initial:end_point);

    Mean(i) = mean(Temp_);
    error(i) = std(Temp_);

end

figure(2011)
% plot(index,data_temp,'ro','MarkerFaceColor','r','MarkerSize',SIZE)
errorbar(Mean,error,'ro','MarkerFaceColor','b','MarkerSize',SIZE)
ylabel ('Temperature [C]',  'FontSize', FT, 'FontName', 'Times')
xlabel ('index',  'FontSize', FT, 'FontName', 'Times')

set(gca,'FontSize',20)

% legend('channel 5','channel 6','Location','southeast')
% title('1 measurement')


 dat = [Mean' error'];
% dat1 = [normalized_time' dataofinterest2'];
% dat2 = normalized_time(images(mm));
writematrix(dat ,'mean_error_channel2', "FileType","text");
```

FIGURE 21: SCRIPT USED TO GET THE ERROR LINES FOR THE TEMPERATURE CALIBRATION.

7.3 Wetting and formation

		Step Label	Number Of Limits	Control Type	Control Value	Extra Control Value 1	Extra Control Value 2
1		Initial rest (wetting)	2	Rest			
	Add Limit			Goto Step	Variable1	Operator1	Value1
	Step Limits		1	Next Step	PV_CHAN_Step_Tim	>=	02:00:00
	Log Limits		2		DV_Time	>=	00:01:00
2		Initial charge to prevent corrosion	2	CCCV	CC(A):0.002	CV(V):1.5	IR(ohm):0
	Add Limit			Goto Step	Variable1	Operator1	Value1
	Step Limits		1	Next Step	PV_CHAN_Step_Tim	>=	04:00:00
	Log Limits		2		DV_Time	>=	00:01:00
3		Rest for further wetting	2	Rest			
	Add Limit			Goto Step	Variable1	Operator1	Value1
	Step Limits		1	Next Step	PV_CHAN_Step_Tim	>=	12:00:00
	Log Limits		2		DV_Time	>=	00:01:00
4		Internal resistance - 1	1	Internal Resistance	Amp:0.005	ms:60.00	Offset:0
	Add Limit			Goto Step	Variable1	Operator1	Value1
	Step Limits		1	Next Step			
5		Initial partial charge	2	C-Rate	0.2		
	Add Limit			Goto Step	Variable1	Operator1	Value1
	Step Limits		1	Rest at partial charge	PV_CHAN_Voltage	>=	3.9
	Log Limits		2		DV_Time	>=	00:00:30
6		Reset capacities - 1	1	Set Variable(s)	Reset	Increment	Decrement
	Add Limit			Goto Step	Variable1	Operator1	Value1
	Step Limits		1	Next Step	PV_CHAN_Step_Tim	>=	00:00:00
7		Rest at partial charge	2	Rest			
	Add Limit			Goto Step	Variable1	Operator1	Value1
	Step Limits		1	Next Step	PV_CHAN_Step_Tim	>=	00:30:00
	Log Limits		2		DV_Time	>=	00:00:30
8		Formation partial/full charge	2	C-Rate	0.2		
	Add Limit			Goto Step	Variable1	Operator1	Value1
	Step Limits		1	Next Step	PV_CHAN_Voltage	>=	4.2
	Log Limits		2		DV_Time	>=	00:00:30
9		Decide to finish formation	3	Rest			
	Add Limit			Goto Step	Variable1	Operator1	Value1
	Step Limits		1	Rest at upper voltage a	TC_Counter1	>=	5
			2	Formation partial disch	TC_Counter1	<	5
	Log Limits		3		DV_Time	>=	00:01:00
10		Formation partial discharge	2	C-Rate	-0.2		
	Add Limit			Goto Step	Variable1	Operator1	Value1
	Step Limits		1	Reset capacities - 1	PV_CHAN_Voltage	<=	3.9
	Log Limits		2		DV_Time	>=	00:00:30
11		Rest at upper voltage after formation	2	Rest			
	Add Limit			Goto Step	Variable1	Operator1	Value1
	Step Limits		1	Next Step	PV_CHAN_Step_Tim	>=	01:00:00
	Log Limits		2		DV_Time	>=	00:00:30
12		Formation complete discharge	2	C-Rate	-0.2		
	Add Limit			Goto Step	Variable1	Operator1	Value1
	Step Limits		1	Next Step	PV_CHAN_Voltage	<	3
	Log Limits		2		DV_Time	>=	00:00:30

FIGURE 22: THE SCHEDULE USED FOR THE WETTING AND FORMATION OF THE BATTERIES.

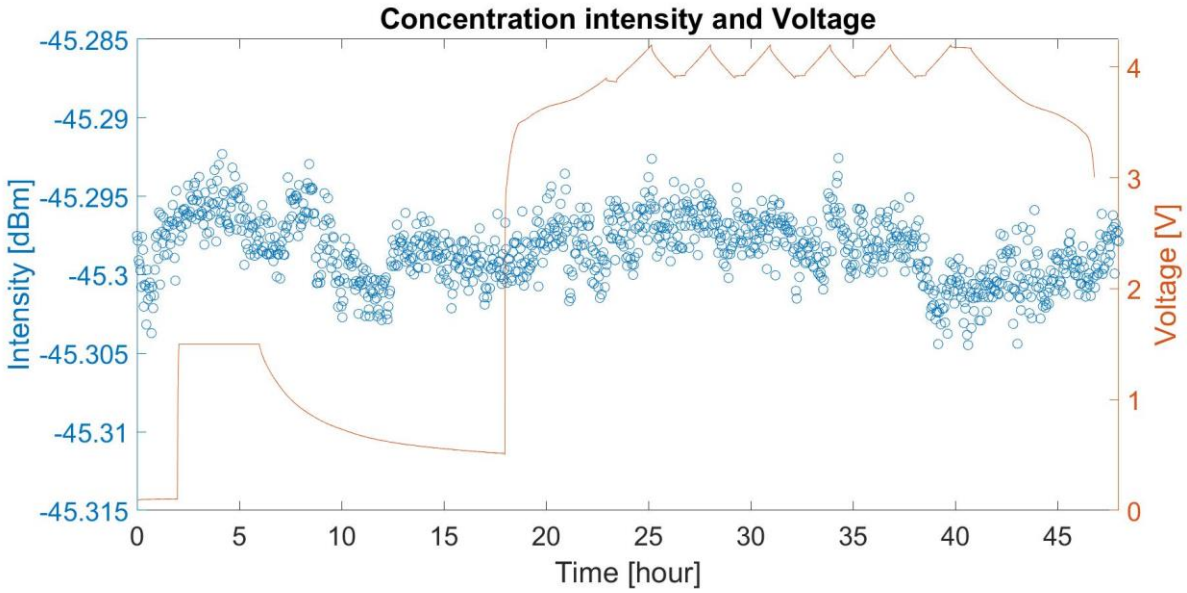

FIGURE 23: AN EXAMPLE OF THE REFLECTED INTENSITY AND THE VOLTAGE – TIME PLOT DURING WETTING AND FORMATION.

7.4 Battery testing

```
close all
clear all
clc

files = dir('D:\Master\TEST7(280723)\TEST7\Responses*.txt');

% only first file
for jj = 1
numlines = 10000;
k = 111;
for i=1:46

m = i-1;
aa= k+18*m;
fileID = fopen(files(jj).name);
thissectionCell = textscan(fileID, '%f', numlines, 'HeaderLines', aa, 'CollectOutput', 1);
data = cell2mat(thissectionCell);
data_mean_channel_2(i) = mean(data);
thissectionCell = textscan(fileID, '%f', numlines, 'HeaderLines', 4, 'CollectOutput', 1);
data = cell2mat(thissectionCell);
data_mean_channel_6(i) = mean(data);
thissectionCell = textscan(fileID, '%f', numlines, 'HeaderLines', 1, 'CollectOutput', 1);
data = cell2mat(thissectionCell);
data_mean_channel_7(i) = mean(data);
thissectionCell = textscan(fileID, '%f', numlines, 'HeaderLines', 6, 'CollectOutput', 1);
data = cell2mat(thissectionCell);
data_mean_channel_13(i) = mean(data);
thissectionCell = textscan(fileID, '%f', numlines, 'HeaderLines', 1, 'CollectOutput', 1);
data = cell2mat(thissectionCell);
data_mean_channel_14(i) = mean(data);
thissectionCell = textscan(fileID, '%f', numlines, 'HeaderLines', 1, 'CollectOutput', 1);
data = cell2mat(thissectionCell);
data_mean_channel_15(i) = mean(data);

fclose('all');
end
% time = 1:length(data_mean_channel_5);
% plot(time,data_mean_channel_5,'o')

end

dat = [data_mean_channel_2' data_mean_channel_6' data_mean_channel_7' data_mean_channel_13' data_mean_channel_14' data_mean_channel_15'];
% dat1 = [normalized_time' dataofinterest2'];
% dat2 = normalized_time(images(mm));
writematrix(dat ,['data_0' num2str(jj)], "FileType","text");
% writematrix(dat1 ,['time_conectivity' namename], "FileType","text");

%% The first 9

close all
clear all
clc

files = dir('D:\Master\TEST7(280723)\TEST7\Responses*.txt');

for jj = 2:9

 numlines = 10000;
% time = 0:10:

k = 2;
for i=1:46
m = i-1;
aa= k+18*m;
fileID = fopen(files(jj).name);
thissectionCell = textscan(fileID, '%f', numlines, 'HeaderLines', aa, 'CollectOutput', 1);
data = cell2mat(thissectionCell);
data_mean_channel_2(i) = mean(data);%(i+46*(jj-1))
thissectionCell = textscan(fileID, '%f', numlines, 'HeaderLines', 4, 'CollectOutput', 1);
data = cell2mat(thissectionCell);
data_mean_channel_6(i) = mean(data);
thissectionCell = textscan(fileID, '%f', numlines, 'HeaderLines', 1, 'CollectOutput', 1);
data = cell2mat(thissectionCell);
data_mean_channel_7(i) = mean(data);
thissectionCell = textscan(fileID, '%f', numlines, 'HeaderLines', 6, 'CollectOutput', 1);
```

FIGURE 24: PART 1 OF THE PROCESSING OF THE RESPONSES FROM THE SENSOR DURING CYCLING OF THE BATTERIES.

```
data = cell2mat(thissectionCell);
data_mean_channel_13(i) = mean(data);
thissectionCell = textscan(fileID, '%f', numlines, 'HeaderLines', 1, 'CollectOutput', 1);
data = cell2mat(thissectionCell);
data_mean_channel_14(i) = mean(data);
thissectionCell = textscan(fileID, '%f', numlines, 'HeaderLines', 1, 'CollectOutput', 1);
data = cell2mat(thissectionCell);
data_mean_channel_15(i) = mean(data);


dat = [data_mean_channel_2' data_mean_channel_6' data_mean_channel_7' data_mean_channel_13' data_mean_channel_14' data_mean_channel_15'];
writematrix(dat ,['data_0' num2str(jj)], "FileType","text");

fclose('all');
end

end

% time = 1:length(data_mean_channel_5);
% plot(time,data_mean_channel_5,'o')

% dat = [data_mean_channel_2' data_mean_channel_6'];
% dat1 = [normalized_time' dataofinterest2'];
% dat2 = normalized_time(images(mm));
% writematrix(dat ,['data_' num2str(jj)], "FileType","text");
% writematrix(dat1 ,['time_conectivity' namename], "FileType","text");
%% Under 100 files

close all
clear all
clc

files = dir('D:\Master\TEST7(280723)\TEST7\Responses*.txt');

for jj = 10:99

 numlines = 10000;
% time = 0:10:

k = 2;
for i=1:46
m = i-1;
aa= k+18*m;
fileID = fopen(files(jj).name);
thissectionCell = textscan(fileID, '%f', numlines, 'HeaderLines', aa, 'CollectOutput', 1);
data = cell2mat(thissectionCell);
data_mean_channel_2(i) = mean(data);%(i+46*(jj-1))
thissectionCell = textscan(fileID, '%f', numlines, 'HeaderLines', 4, 'CollectOutput', 1);
data = cell2mat(thissectionCell);
data_mean_channel_6(i) = mean(data);
thissectionCell = textscan(fileID, '%f', numlines, 'HeaderLines', 1, 'CollectOutput', 1);
data = cell2mat(thissectionCell);
data_mean_channel_7(i) = mean(data);
thissectionCell = textscan(fileID, '%f', numlines, 'HeaderLines', 6, 'CollectOutput', 1);
data = cell2mat(thissectionCell);
data_mean_channel_13(i) = mean(data);
thissectionCell = textscan(fileID, '%f', numlines, 'HeaderLines', 1, 'CollectOutput', 1);
data = cell2mat(thissectionCell);
data_mean_channel_14(i) = mean(data);
thissectionCell = textscan(fileID, '%f', numlines, 'HeaderLines', 1, 'CollectOutput', 1);
data = cell2mat(thissectionCell);
data_mean_channel_15(i) = mean(data);


dat = [data_mean_channel_2' data_mean_channel_6' data_mean_channel_7' data_mean_channel_13' data_mean_channel_14' data_mean_channel_15'];
writematrix(dat ,['data_' num2str(jj)], "FileType","text");

fclose('all');
end

end

% time = 1:length(data_mean_channel_5);
% plot(time,data_mean_channel_5,'o')
```

FIGURE 25: PART 2 OF THE PROCESSING OF THE RESPONSES FROM THE SENSOR DURING CYCLING OF THE BATTERIES.

```
% dat = [data_mean_channel_2' data_mean_channel_6'];
% dat1 = [normalized_time' dataofinterest2'];
% dat2 = normalized_time(images(mm));
% writematrix(dat ,['data_' num2str(jj)], "FileType","text");
% writematrix(dat1 ,['time_conectivity' namename], "FileType","text");
%% Above 100 files

close all
clear all
clc

files = dir('D:\Master\TEST7(280723)\TEST7\Responses*.txt');

for jj = 100:403

 numlines = 10000;
% time = 0:10:

k = 2;
for i=1:46
m = i-1;
aa= k+18*m;
fileID = fopen(files(jj).name);
thissectionCell = textscan(fileID, '%f', numlines, 'HeaderLines', aa, 'CollectOutput', 1);
data = cell2mat(thissectionCell);
data_mean_channel_2(i) = mean(data);%(i+46*(jj-1))
thissectionCell = textscan(fileID, '%f', numlines, 'HeaderLines', 4, 'CollectOutput', 1);
data = cell2mat(thissectionCell);
data_mean_channel_6(i) = mean(data);
thissectionCell = textscan(fileID, '%f', numlines, 'HeaderLines', 1, 'CollectOutput', 1);
data = cell2mat(thissectionCell);
data_mean_channel_7(i) = mean(data);
thissectionCell = textscan(fileID, '%f', numlines, 'HeaderLines', 6, 'CollectOutput', 1);
data = cell2mat(thissectionCell);
data_mean_channel_13(i) = mean(data);
thissectionCell = textscan(fileID, '%f', numlines, 'HeaderLines', 1, 'CollectOutput', 1);
data = cell2mat(thissectionCell);
data_mean_channel_14(i) = mean(data);
thissectionCell = textscan(fileID, '%f', numlines, 'HeaderLines', 1, 'CollectOutput', 1);
data = cell2mat(thissectionCell);
data_mean_channel_15(i) = mean(data);


dat = [data_mean_channel_2' data_mean_channel_6' data_mean_channel_7' data_mean_channel_13' data_mean_channel_14' data_mean_channel_15'];
writematrix(dat ,['data__' num2str(jj)], "FileType","text");

fclose('all');
end

end

% time = 1:length(data_mean_channel_5);
% plot(time,data_mean_channel_5,'o')

% dat = [data_mean_channel_2' data_mean_channel_6'];
% dat1 = [normalized_time' dataofinterest2'];
% dat2 = normalized_time(images(mm));
% writematrix(dat ,['data_' num2str(jj)], "FileType","text");
% writematrix(dat1 ,['time_conectivity' namename], "FileType","text");

%%

close all
clear all
clc

figure(1)
SIZE = 5;
files = dir('D:\Master\TEST7(280723)\TEST7\data*.txt');
data_to_plot = [];
data_to_plot_1 = [];
data_to_plot_2 = [];
data_to_plot_3 = [];
```

FIGURE 26: PART 3 OF THE PROCESSING OF THE RESPONSES FROM THE SENSOR DURING CYCLING OF THE BATTERIES.

```
data_to_plot_4 = [];
data_to_plot_5 = [];
for i=1:length(files)

final_data = importdata(files(i).name);

channel_2 = (final_data(:,1));
channel_6 = (final_data(:,2));
channel_7 = (final_data(:,3));
channel_13 = (final_data(:,4));
channel_14 = (final_data(:,5));
channel_15 = (final_data(:,6));
data_to_plot=cat(1,data_to_plot,channel_2);
data_to_plot_1=cat(1,data_to_plot_1,channel_6);
data_to_plot_2=cat(1,data_to_plot_2,channel_7);
data_to_plot_3=cat(1,data_to_plot_3,channel_13);
data_to_plot_4=cat(1,data_to_plot_4,channel_14);
data_to_plot_5=cat(1,data_to_plot_5,channel_15);
% data_to_plot = [data_to_plot channel_5];
end
time = 1:length(data_to_plot);
real_time = (time*10)/60;
mm = 1;
plot(real_time(1:mm:end),data_to_plot(1:mm:end),'ro','MarkerFaceColor','r','MarkerSize',SIZE)
hold on
%plot(real_time(1:mm:end),data_to_plot_1(1:mm:end),'bo','MarkerFaceColor','b','MarkerSize',SIZE)
% plot(real_time(1:mm:end),data_to_plot_2(1:mm:end),'go','MarkerFaceColor','g','MarkerSize',SIZE)


FT = 15;
ylabel ('Intesity [dBm]',  'FontSize', FT, 'FontName', 'Times')
xlabel ('Time [min]',  'FontSize', FT, 'FontName', 'Times')

% axis ([0 1200 0 100])
set(gca,'FontSize',20)

% legend('channel 2')%,'channel 6')%,'Location','northwest')
title('Exp1')

%% Write text file of all data

dat = [data_to_plot data_to_plot_1 data_to_plot_2 data_to_plot_3 data_to_plot_4 data_to_plot_5];
% dat1 = [normalized_time' dataofinterest2'];
% dat2 = normalized_time(images(mm));
writematrix(dat ,'data_full_experiment', "FileType","text");

```

FIGURE 27: PART 4 OF THE PROCESSING OF THE RESPONSES FROM THE SENSOR DURING CYCLING OF THE BATTERIES.

```
%% Define Arbin data input (import as table)
% Arbindata = minipouchLFPfull; % struct/table (if manual import)
[filename,path]=uigetfile('*.csv','SELECT ARBIN FILE','D:\Master\TEST7(280723)\TEST7');
fullFileName=fullfile(path, filename); %char(strcat(path,filename));
Arbindata = readtable(fullFileName);
% And these to fix the time vector
time_arbin = Arbindata.DateTime; % date/time
ax=hours(time_arbin-time_arbin(1));
%%
voltage =  Arbindata.Voltage_V_;
SIZE = 10;

figure(1)
clf
plot(ax,voltage,'r-','MarkerFaceColor','r','MarkerSize',SIZE)
hold on
FT = 15;
ylabel ('Voltage [V]',  'FontSize', FT, 'FontName', 'Times')
xlabel ('Time [hour]',  'FontSize', FT, 'FontName', 'Times')
set(gca,'FontSize',20)
% axis([10 80 2.85 4.25])
title('Voltage readout')
%%
SIZE = 7;
concentration = importdata("data_full_experiment.txt");
concentration_channel_2=concentration(:,1);
concentration_channel_6=concentration(:,2);
concentration_channel_7=concentration(:,3);
concentration_channel_13=concentration(:,4);
concentration_channel_14=concentration(:,5);
concentration_channel_15=concentration(:,6);
time_step = 2*60 + 30;
final_time = (length(concentration_channel_2)-1)*time_step;
time = 0:time_step:final_time;
time = time/(60*60);

figure(2)
clf
plot(time,concentration_channel_2,'bo','MarkerFaceColor','b','MarkerSize',SIZE)
hold on
FT = 15;
ylabel ('Intensity [dBm]',  'FontSize', FT, 'FontName', 'Times')
xlabel ('Time [hour]',  'FontSize', FT, 'FontName', 'Times')
set(gca,'FontSize',20)
%axis([10 80 -31.26 -31.2])
title('Concentration readout')
%% 2 axis plot

figure(3)
clf
x = ax;
y = voltage;
% yyaxis left
% plot(time,concentration_channel_2,'o','MarkerSize',SIZE);
% ylabel ('Intensity [dB]',  'FontSize', FT, 'FontName', 'Times')
% xlabel ('Time [hour]',  'FontSize', FT, 'FontName', 'Times')
% set(gca,'FontSize',20)
%
% hold on
%
% yyaxis left
% plot(time,concentration_channel_6,'o','MarkerSize',SIZE);
% ylabel ('Intensity [dB]',  'FontSize', FT, 'FontName', 'Times')
% xlabel ('Time [hour]',  'FontSize', FT, 'FontName', 'Times')
% set(gca,'FontSize',20)
% %
% hold on
%
% yyaxis left
% plot(time,concentration_channel_7,'o','MarkerSize',SIZE);
% ylabel ('Intensity [dB]',  'FontSize', FT, 'FontName', 'Times')
% xlabel ('Time [hour]',  'FontSize', FT, 'FontName', 'Times')
% set(gca,'FontSize',20)
%
% hold on
```

FIGURE 28: PART 1 OF THE SCRIPT TO GENERATE THE PLOTS FOR BATTERY TESTING.

```
%
% yyaxis left
% plot(time,concentration_channel_13,'o','MarkerSize',SIZE);
% ylabel ('Intensity [dB]',  'FontSize', FT, 'FontName', 'Times')
% xlabel ('Time [hour]',  'FontSize', FT, 'FontName', 'Times')
% set(gca,'FontSize',20)
%
% hold on
%
yyaxis left
plot(time,concentration_channel_14,'o','MarkerSize',SIZE);
ylabel ('Intensity [dB]',  'FontSize', FT, 'FontName', 'Times')
xlabel ('Time [hour]',  'FontSize', FT, 'FontName', 'Times')
set(gca,'FontSize',20)

%  axis([160.4 292.58 -31.26 -31.22])

% hold on
%
% yyaxis left
% plot(time,concentration_channel_15,'o','MarkerSize',SIZE);
% ylabel ('Intensity [dB]',  'FontSize', FT, 'FontName', 'Times')
% xlabel ('Time [hour]',  'FontSize', FT, 'FontName', 'Times')
% set(gca,'FontSize',20)

% axis([10 80 -31.26 -31.2])

yyaxis right
plot(x,y);
FT = 15;
ylabel ('Voltage [V]',  'FontSize', FT, 'FontName', 'Times')
xlabel ('Time [hour]',  'FontSize', FT, 'FontName', 'Times')
set(gca,'FontSize',20)



% axis([160.4 292.58 2.85 4.25])
% axis([551 767 2.85 4.25])
% axis([10 163 2.85 4.25])
% axis([22 130 2.85 4.25])
% axis([158 163 2.85 4.25])
% axis([161.84 161.866 2.85 4.25])
axis([0 10 2.85 4.25])


yyaxis left
% title('Concentration intensity and Voltage (channel 13)')
xlabel('Time [hour]')
ylabel('Intensity [dBm]')

yyaxis right
ylabel('Voltage [V]')
```

FIGURE 29: PART 2 OF THE SCRIPT TO GENERATE THE PLOTS FOR BATTERY TESTING.

		Step Label	Number Of Limits	Control Type	Control Value	Extra Control Value 1	Extra Control Value 2
1		Initial rest - stabilizing	2	Rest			
		Add Limit		Goto Step	Variable1	Operator1	Value1
		Step Limits	1	Internal resistance for tester	PV_CHAN_Step_Time	>=	00:00:30
		Log Limits	2		DV_Time	>=	00:00:30
2		Internal resistance for tester	1	Internal Resistance	Amp:0.005	ms:60.00	Offset:0
		Add Limit		Goto Step	Variable1	Operator1	Value1
		Step Limits	1	Next Step			
3		Initial CCCV charge	2	CCCV	CC(A):0.2	CV(V):MV_UD3	IR(ohm):0
		Add Limit		Goto Step	Variable1	Operator1	Value1
		Step Limits	1	Next Step	PV_CHAN_Current	<=	0.01
		Log Limits	2		DV_Time	>=	00:01:00
4		Rest at upper voltage before C/20	2	Rest			
		Add Limit		Goto Step	Variable1	Operator1	Value1
		Step Limits	1	Next Step	PV_CHAN_Step_Time	>=	02:00:00
		Log Limits	2		DV_Time	>=	00:02:00
5		Reset capacities - 1	1	Set Variable(s)	Reset	Increment	Decrement
		Add Limit		Goto Step	Variable1	Operator1	Value1
		Step Limits	1	Next Step	PV_CHAN_Step_Time	>=	00:00:00
6		Discharge at C/20	2	C-Rate	-0.05		
		Add Limit		Goto Step	Variable1	Operator1	Value1
		Step Limits	1	Next Step	PV_CHAN_Voltage	<=	MV_UD2
		Log Limits	2		DV_Time	>=	00:01:00
7		Rest at lower voltage - C/20	2	Rest			
		Add Limit		Goto Step	Variable1	Operator1	Value1
		Step Limits	1	Next Step	PV_CHAN_Step_Time	>=	00:15:00
		Log Limits	2		DV_Time	>=	00:00:30
8		Charge at C/20	2	C-Rate	0.05		
		Add Limit		Goto Step	Variable1	Operator1	Value1
		Step Limits	1	Next Step	PV_CHAN_Voltage	>=	4.2
		Log Limits	2		DV_Time	>=	00:01:00
9		Rest at upper voltage - C/20	2	Rest			
		Add Limit		Goto Step	Variable1	Operator1	Value1
		Step Limits	1	Next Step	PV_CHAN_Step_Time	>=	00:15:00
		Log Limits	2		DV_Time	>=	00:00:30
10		Internal resistance for tester - C/20	1	Internal Resistance	Amp:0.005	ms:60.00	Offset:0
		Add Limit		Goto Step	Variable1	Operator1	Value1
		Step Limits	1	Next Step			
11		Decision to proceed with C/10	2	Set Variable(s)	Reset	Increment	Decrement
		Add Limit		Goto Step	Variable1	Operator1	Value1
		Step Limits	1	Discharge at C/20	TC_Counter1	<	2
			2	Next Step	TC_Counter1	>=	2
12		Pause until further notice - now rest	1	Rest			
		Add Limit		Goto Step	Variable1	Operator1	Value1
		Step Limits	1	Next Step	PV_CHAN_Step_Time	>=	00:00:30
13		Discharge at C/10	2	C-Rate	-0.1		
		Add Limit		Goto Step	Variable1	Operator1	Value1
		Step Limits	1	Next Step	PV_CHAN_Voltage	<=	MV_UD2
		Log Limits	2		DV_Time	>=	00:01:00
14		Rest at lower voltage - C/10	2	Rest			
		Add Limit		Goto Step	Variable1	Operator1	Value1
		Step Limits	1	Next Step	PV_CHAN_Step_Time	>=	00:15:00
		Log Limits	2		DV_Time	>=	00:00:30
15		Charge at C/10	2	CCCV	CC(A):0.02	CV(V):4.2	IR(ohm):0
		Add Limit		Goto Step	Variable1	Operator1	Value1
		Step Limits	1	Next Step	PV_CHAN_Current	<=	0.01
		Log Limits	2		DV_Time	>=	00:01:00
16		Rest at upper voltage - C/10	2	Rest			
		Add Limit		Goto Step	Variable1	Operator1	Value1
		Step Limits	1	Next Step	PV_CHAN_Step_Time	>=	00:15:00
		Log Limits	2		DV_Time	>=	00:00:30
17		Internal resistance for tester - C/10	1	Internal Resistance	Amp:0.005	ms:1.00	Offset:0
		Add Limit		Goto Step	Variable1	Operator1	Value1
		Step Limits	1	Next Step			
18		Decision to proceed with C/2	2	Set Variable(s)	Reset	Increment	Decrement
		Add Limit		Goto Step	Variable1	Operator1	Value1
		Step Limits	1	Discharge at C/10	TC_Counter2	<	3
			2	Next Step	TC_Counter2	>=	3
19		Pause until further notice - 2	1	Rest			
		Add Limit		Goto Step	Variable1	Operator1	Value1
		Step Limits	1	Next Step	PV_CHAN_Step_Time	>=	00:00:30
20		Discharge at C/2	2	C-Rate	-0.5		
		Add Limit		Goto Step	Variable1	Operator1	Value1
		Step Limits	1	Next Step	PV_CHAN_Voltage	<=	MV_UD2
		Log Limits	2		DV_Time	>=	00:01:00
21		Rest at lower voltage - C/2	2	Rest			
		Add Limit		Goto Step	Variable1	Operator1	Value1
		Step Limits	1	Next Step	PV_CHAN_Step_Time	>=	00:15:00
		Log Limits	2		DV_Time	>=	00:00:30
22		Charge at C/2	2	CCCV	CC(A):0.1	CV(V):4.2	IR(ohm):0
		Add Limit		Goto Step	Variable1	Operator1	Value1
		Step Limits	1	Next Step	PV_CHAN_Current	<=	0.01
		Log Limits	2		DV_Time	>=	00:01:00
23		Rest at upper voltage - C/2	2	Rest			
		Add Limit		Goto Step	Variable1	Operator1	Value1
		Step Limits	1	Next Step	PV_CHAN_Step_Time	>=	00:15:00
		Log Limits	2		DV_Time	>=	00:00:30
24		Internal resistance for tester - C/2	1	Internal Resistance	Amp:0	ms:1.00	Offset:0
		Add Limit		Goto Step	Variable1	Operator1	Value1
		Step Limits	1	Next Step			
25		Descision to proceed with C/2	2	Set Variable(s)	Reset	Increment	Decrement
		Add Limit		Goto Step	Variable1	Operator1	Value1
		Step Limits	1	Discharge at C/2	TC_Counter1	<	5
			2	Next Step	TC_Counter1	>=	5
26		Pause until further motice - C/2	1	Rest			
		Add Limit		Goto Step	Variable1	Operator1	Value1
		Step Limits	1	Next Step	PV_CHAN_Step_Time	>=	00:00:30
27		Discharge at 1 C	2	C-Rate	-1		

FIGURE 30: PART 1 OF THE FULL SCHEDULE OF THE BATTERY TESTING.

	Add Limit			Goto Step	Variable1	Operator1	Value1
	Step Limits		1	Next Step	PV_CHAN_Voltage	<=	MV_UD2
	Log Limits		2		DV_Time	>=	00:01:00
28		Rest at lower voltage (1C)	2	Rest			
	Add Limit			Goto Step	Variable1	Operator1	Value1
	Step Limits		1	Next Step	PV_CHAN_Step_Time	>=	00:15:00
	Log Limits		2		DV_Time	>=	00:00:30
29		Charge at 1 C	2	CCCV	CC(A):0.2	CV(V):4.2	IR(ohm):0
	Add Limit			Goto Step	Variable1	Operator1	Value1
	Step Limits		1	Next Step	PV_CHAN_Current	<=	0.01
	Log Limits		2		DV_Time	>=	00:01:00
30		Rest at upper voltage (1C)	2	Rest			
	Add Limit			Goto Step	Variable1	Operator1	Value1
	Step Limits		1	Next Step	PV_CHAN_Step_Time	>=	00:15:00
	Log Limits		2		DV_Time	>=	00:00:30
31		Internal resisistance for tester - 1 C	1	Internal Resistance	Amp:0.005	ms:60.00	Offset:0
	Add Limit			Goto Step	Variable1	Operator1	Value1
	Step Limits		1	Next Step			
32		Decison to proceed with 2 C	2	Set Variable(s)	Reset	Increment	Decrement
	Add Limit			Goto Step	Variable1	Operator1	Value1
	Step Limits		1	Discharge at 1 C	TC_Counter3	<	5
			2	Next Step	TC_Counter3	>=	5
33		Pause until furter notice - 6 (now rest)	1	Rest			
	Add Limit			Goto Step	Variable1	Operator1	Value1
	Step Limits		1	Next Step	PV_CHAN_Step_Time	>=	00:00:30
34		Discharge at 2 C	2	C-Rate	-2		
	Add Limit			Goto Step	Variable1	Operator1	Value1
	Step Limits		1	Next Step	PV_CHAN_Voltage	>=	MV_UD2
	Log Limits		2		DV_Time	>=	00:01:00
35		Rest at lower voltage - 2 C	2	Rest			
	Add Limit			Goto Step	Variable1	Operator1	Value1
	Step Limits		1	Next Step	PV_CHAN_Step_Time	>=	00:15:00
	Log Limits		2		DV_Time	>=	00:00:30
36		Charge (2 C)	2	CCCV	CC(A):0.4	CV(V):4.2	IR(ohm):0
	Add Limit			Goto Step	Variable1	Operator1	Value1
	Step Limits		1	Next Step	PV_CHAN_Current	<=	0.01
	Log Limits		2		DV_Time	>=	00:01:00
37		Rest at upper voltage (2 C)	2	Rest			
	Add Limit			Goto Step	Variable1	Operator1	Value1
	Step Limits		1	Next Step	PV_CHAN_Step_Time	>=	00:15:00
	Log Limits		2		DV_Time	>=	00:00:30
38		Internal resistance for tester - 2 C	1	Internal Resistance	Amp:0.005	ms:60.00	Offset:0
	Add Limit			Goto Step	Variable1	Operator1	Value1
	Step Limits		1	Next Step			
39		Decision to proceed with 3 C	2	Set Variable(s)	Reset	Increment	Decrement
	Add Limit			Goto Step	Variable1	Operator1	Value1
	Step Limits		1	Discharge at 2 C	TC_Counter4	<	5
			2	Next Step	TC_Counter4	>=	5
40		Pause until further notice - 3 C	1	Rest			
	Add Limit			Goto Step	Variable1	Operator1	Value1
	Step Limits		1	Next Step	PV_CHAN_Step_Time	>=	00:00:30
41		Discharge at 3 C	2	C-Rate	-3		
	Add Limit			Goto Step	Variable1	Operator1	Value1
	Step Limits		1	Next Step	PV_CHAN_Voltage	>=	MV_UD2
	Log Limits		2		DV_Time	>=	00:01:00
42		Rest at lower voltage - 3 C	2	Rest			
	Add Limit			Goto Step	Variable1	Operator1	Value1
	Step Limits		1	Next Step	PV_CHAN_Step_Time	>=	00:15:00
	Log Limits		2		DV_Time	>=	00:00:30
43		Charge (3 C)	2	CCCV	CC(A):0.6	CV(V):4.2	IR(ohm):0
	Add Limit			Goto Step	Variable1	Operator1	Value1
	Step Limits		1	Next Step	PV_CHAN_Current	<=	0.01
	Log Limits		2		DV_Time	>=	00:01:00
44		Rest at upper voltage (3 C)	2	Rest			
	Add Limit			Goto Step	Variable1	Operator1	Value1
	Step Limits		1	Next Step	PV_CHAN_Step_Time	>=	00:15:00
	Log Limits		2		DV_Time	>=	00:00:30
45		Internal resistance for tester - 3 C	1	Internal Resistance	Amp:0.005	ms:60.00	Offset:0
	Add Limit			Goto Step	Variable1	Operator1	Value1
	Step Limits		1	Next Step			
46		Decision to proceed with C/20	2	Set Variable(s)	Reset	Increment	Decrement
	Add Limit			Goto Step	Variable1	Operator1	Value1
	Step Limits		1	Discharge at 3 C	TC_Counter1	<	5
			2	Next Step	TC_Counter1	>=	5
47		Pause until further notice - C/20	1	Rest			
	Add Limit			Goto Step	Variable1	Operator1	Value1
	Step Limits		1	Next Step	PV_CHAN_Step_Time	>=	00:00:30
48		Repeat	2	Set Variable(s)	Reset	Increment	Decrement
	Add Limit			Goto Step	Variable1	Operator1	Value1
	Step Limits		1	Discharge at C/20	TC_Counter2	<	2
			2	Next Step	TC_Counter2	>=	2
49		Final discharge	2	C-Rate	-0.5		
	Add Limit			Goto Step	Variable1	Operator1	Value1
	Step Limits		1	Next Step	PV_CHAN_Voltage	>=	MV_UD2
	Log Limits		2		DV_Time	>=	00:01:00
50		Final rest	2	Rest			
	Add Limit			Goto Step	Variable1	Operator1	Value1
	Step Limits		1	End Test	PV_CHAN_Step_Time	>=	10:00:00
	Log Limits		2		DV_Time	>=	00:01:00

FIGURE 31: PART 2 OF THE FULL SCHEDULE OF THE BATTERY TESTING.